DESIGN AND OPTIMISATION OF NEW BEAMLINES FOR iTHEMBA LABORATORY FOR ACCELERATOR BASED SCIENCES (iThemba LABS)

Pogisho Mokgasi Maine

Supervisor: Dr. J. L. Conradie
Co-supervisor: Mr. D. T. Fourie

Dissertation submitted in fulfillment of the requirements for the degree of
Masters of Science in Applied Radiation Science and Technology

Centre for Applied Radiation Science and Technology,
Faculty of Agriculture Science and Technology,
University of North-West,
Republic of South Africa,
March 2002

DESIGN AND OPTIMISATION OF NEW BEAMLINES FOR iTHEMBA LABORATORY FOR ACCELERATOR BASED SCIENCES (iThemba LABS)

POGISHO MOKGASI MAINE

iThemba LABS, P.O. Box 722, Somerset West 7129, Republic of South Africa

March 2002

ABSTRACT

The facilities at iThemba LABS are used for basic and applied research, treatment of patients with proton and neutron beams and the production of radioisotopes for hospitals and industry. The laboratory operates a 6 MV Van de Graaff accelerator and three cyclotrons. The cyclotron complex comprises of the two injector cyclotrons: the light-ion solid-pole injector cyclotron (SPC1) and the second solid-pole injector cyclotron (SPC2) which pre-accelerate and inject beams of particles into the large separated-sector cyclotron (SSC), which accelerates the particles up to a maximum energy of 200 MeV for protons. SPC1 uses an internal Penning Ionization Gauge (PIG) ion source that provides beams of light ions. SPC2 has two external ion sources; the polarized ion source and an electron cyclotron resonance (ECR) ion source, which provides beams of polarized hydrogen ions and heavy ions, respectively.

In addition to the existing two external ion sources a third ion source, for acceleration of high intensity beams of protons, is being planned for SPC2. The new source, which will also be external to SPC2, has to inject a beam into one of the existing injection beamlines of SPC2. A suitable position for coupling the ion source to the injection beamlines of SPC2 has been found and in order to match the beam from the source to the existing lines a short new beamline section has been designed. A double focusing 90^0 bending magnet, for separation of the proton beam from unwanted molecular hydrogen ions has to be inserted between the source and the existing beamlines. Because of space limitations the bending magnet will also be used to focus the beam in both the horizontal and vertical directions. By calculation, using the computer program TRANSPORT, the best position for the ion source with

respect to the magnet, and the optimum entrance and exit edge angles of 34.7^0 for the magnet, have been determined. Satisfactory beam envelopes could be obtained with the existing beamline elements up to the centre of SPC2. This shows that except for the bending magnet no further beamline elements are required to inject a beam from the new source into SPC2. Approximate analytical expressions were used to design and optimize the dimensions of the 90^0 bending magnet. An H-type magnet with a bending radius of 220 mm and a pole gap of 70 mm were decided upon. More accurate field calculations performed with the commercially available computer program TOSCA, which uses finite element analysis, verified the results obtained with analytical expressions. Saturation effects are negligible even at higher than required excitation of the coil and the field homogeneity in the beam region between the pole plates is better than 2% of the maximum field value.

With the current design of the beamlines at the Van de Graaff accelerator, which dates back to 1962, the energy resolution is poor. Initially there was no need for higher energy resolution, but in recent years, with the acquisition of the multi-probe facility and the stronger emphasis on solid state physics experiments, the demand for beams with high energy-resolution increased. To obtain high energy resolution in a beamline at least one double-focusing bending magnet, with a large radius, as well as object and image slits, on which the beam should be focused, are required. The Van de Graaff beamlines were redesigned to improve their energy resolution and the quality of the beams delivered to the different users. Calculations, using the computer program TRANSPORT and emittance data obtained by fitting measured to calculated beam profiles, have shown that with two additional quadrupole magnets, an additional slit and modification of the entrance and exit edge angles of the existing 90^0 bending magnet in the beamline, the energy resolution can be improved from 1% to 0.15%. This modification will not only result in better energy resolution but also in improved transmission efficiency in all the beamlines. Consequently, beams of adequate intensity and quality will become available when these modifications are implemented.

ACKNOWLEDGEMENTS

I would like to take this opportunity to thank everyone who offered advice and assistance during the research period especially my supervisor at iThemba LABS, Dr. J.L. Conradie, for his excellent supervision and encouragement.

I am also indebted to:

- Mr. D.T. Fourie for assisting with the computer program TRANSPORT related skills and always being there when I needed help.

- Mr. K.A. Springhorn for helping in emittance measurements performed at the Van de Graaff accelerator of iThemba LABS and his willingness and valuable support.

- Mr. J.L.G. Delsink for assisting in measurements taking of the Van de Graaff accelerator and of the beamline between the duoplasmatron ion source and SPC2, as well as for providing layout diagrams of iThemba LABS.

- Mr. J.G. de Villiers for calculations with the computer program TOSCA and the diagrams of the bending magnet.

- The staff of accelerator group of iThemba LABS for their assistance and support.

I furthermore acknowledge the financial support from the National Research Foundation (NRF) and the opportunity for using the facilities of iThemba LABS. I would like to extend my word of thanks to the University of North-West (UNW) through the Centre for Applied Radiation Science and Technology (CARST) for allowing me to undertake this project.

I am grateful for support and encouragement I received from my colleagues and friends.

Finally, I would like to thank my family for their patience, support, comfort, encouragement and love.

TABLE OF CONTENTS

CHAPTER 1

MOTIVATION AND OUTLINE

1.1 INTRODUCTION

iThemba Laboratory for Accelerator Based Sciences, iThemba LABS, is a national research facility [**NAC76**] which provides beams of energetic charged particles and facilities for research and training. This multi-disciplinary scientific research institute further serves the national community by conducting basic and applied research, providing facilities for particle radiotherapy treatment of patients with proton and neutron beams on site, producing radioisotopes for hospitals and industry and by the training of students in a wide range of fields.

iThemba LABS operate a 6 MV Van de Graaff accelerator and three cyclotrons. The cyclotron complex comprises of the two injector cyclotrons: the light-ion solid-pole injector cyclotron (SPC1) and the second solid-pole injector cyclotron (SPC2) that pre-accelerate and feed beams of particles into the large main separated-sector cyclotron (SSC), which accelerates the particles up to high energies. SPC1 uses an internal Penning Ionisation Gauge (PIG) ion source that provides beams of light ions. SPC2 has two external ion sources, the polarised ion source and an electron cyclotron resonance (ECR) ion source, which provides beams of polarised hydrogen ions and heavy ions, respectively.

Radioisotopes and radio-pharmaceuticals are produced using an intense 66 MeV proton beam from the SSC with SPC1 as injector. The same beam is also used for the production of neutrons for therapy, using the facilities provided by the iThemba LABS' Medical Radiation Division. For protontherapy, protons are accelerated to 200 MeV in the SSC, also with SPC1 as injector cyclotron. Beams of both light and heavy ions from the separated-sector cyclotron are utilized for nuclear physics research.

1.2 MOTIVATION FOR THIS STUDY

The objectives of this project are:

- The design and optimisation of a beamline from a third external ion source to the centre of the second solid-pole injector cyclotron, using beam transport calculations. The emittance of the beam delivered by a newly developed duoplasmatron ion source will be used as a starting condition for the beam optics calculations, using the well-known beam optics program TRANSPORT **[CAR98]**. This ion source and beamline will be used for acceleration of high intensity proton beams with SPC2. Proton beams from SPC2 are required for isotope production and proton- and neutrontherapy when the light-ion injector cyclotron is out of operation. With the new source and beamline the reliability of beam delivery for these important applications will be improved considerably. The design of a 90^0 dipole magnet needed for this new beamline, will be based on calculations using approximate analytical expressions and more accurate calculations with the computer program TOSCA.

- The beamlines of the Van de Graaff accelerator at iThemba LABS will be redesigned to increase their energy resolution and therefore the quality of the beams delivered to users.

- The design method and characteristics of the beamlines that is established in this report will not only be applicable to the Van de Graaff accelerator and the beamline of the second solid-pole injector cyclotron of iThemba LABS, but can generally be applied to accelerators of a similar nature.

1.3 OUTLINE OF THESIS

This thesis is structured as follows:

- The facilities at iThemba LABS are briefly presented in chapter 2 with the main emphasis on the Van de Graaff accelerator and SPC2.

- The mathematical beam transport formalism for beam lines will be introduced in chapter 3. The sigma-matrix formalism and first order matrix calculations will be emphasised.

- Chapter 4 briefly describes the most important beam transport elements and their matrix treatment.

- The design of the beamline between the external duoplasmatron ion source and SPC2 will be considered in chapter 5. In addition, the injection of the beam from the source into the SPC2 will be described.

- The design optimisation of the dipole magnet and its energy resolution will be discussed in chapter 6. The computer program TOSCA will be used for the design.

- The emittance measurements and the redesign of the Van de Graaff accelerator beamlines will be discussed in chapter 7.

- Finally, the conclusions of this study are presented in chapter 8.

CHAPTER 2

ACCELERATOR FACILITIES AT iTHEMBA LABORATORY FOR ACCELERATOR BASED SCIENCES (iThemba LABS)

2.1 INTRODUCTION

During the early nineteen seventies nuclear physicists and radiotherapists in South Africa were considering the acquisition of new accelerator facilities for their respective disciplines. Because of a lack of funds they decided that it would be best to pool available resources together to create a single national multi-disciplinary facility, which would meet the requirements for nuclear physics, particle radiotherapy and the production of radioisotopes, for South Africa. The main accelerator facilities in operation at that stage in South Africa were the locally built variable energy CSIR cyclotron, capable of accelerating alpha particles to 34 MeV, deuterons to 17 MeV, protons to 15.3 MeV and Helium-3 ions to 39 MeV, and the 6 MV Van de Graaff accelerator of the Southern Universities Nuclear Institute, SUNI. A feasibility study **[NAC76]**, which led to establishment of the National Accelerator Centre (NAC) with a 200 MeV separated-sector cyclotron as the main accelerator, was carried out. The project was approved in 1977 and protons were first accelerated up to the extraction radius of the SSC in October 1985. In due time the Southern Universities Nuclear Institute was incorporated in the National Accelerator Centre, which later became iThemba LABS. Experience gained with the design, construction and development of the CSIR cyclotron and the unique requirements of the multi-disciplinary facility led to the decision to design and built the 200 MeV cyclotron and the two injector cyclotrons in South Africa. This proved to be a wise decision since not only were machines of excellent quality designed and built in a relatively short time but irreplaceable experience was gained in the process. It also had the advantage that the staff, who later on had to operate, maintain and develop the cyclotrons and other facilities, were experienced people with intimate knowledge of the machines that they designed and built themselves.

2.2 LAYOUT OF THE CYLOTRON FACILITIES

The current layout of the iThemba LABS cyclotron facilities is shown in figure 2.1. Two injector cyclotrons, a K = 8 MeV cyclotron, SPC1, for acceleration of light-ion beams, and a K = 10 MeV cyclotron, SPC2, for acceleration of polarized hydrogen and heavy ions, deliver pre-accelerated beams to the main cyclotron, a K = 200 MeV SSC.

The SSC accelerates beams of both light and heavy ions to a maximum energy of 200 MeV for protons. The beam is extracted from the SSC and directed to the user areas and vaults for isotope production, neutron- and protontherapy and nuclear physics and radiobiology research.

Between the cyclotrons and from the SSC to the user areas the beam moves through evacuated stainless-steel pipes. The main elements of the beamlines are the quadrupole magnets, positioned around the beam pipes, for beam focussing and the dipole magnets for changing the beam direction as well as for focussing. At low energies, such as in the beamline between the external ion sources and SPC2, solenoids are also used for focussing. Longitudinal focussing, and compensation for spread out of the beam due to energy spread, is compensated for with beam bunchers.

Presently, the establishment of a Major Radiation Medicine Centre (MRMC) at iThemba LABS, that will comprise of its own 230 MeV cyclotron for proton therapy, is being considered. After its construction, the existing SSC will no longer be overtaxed and this means more beam time will be available for the production of radionuclides and physics experiments.

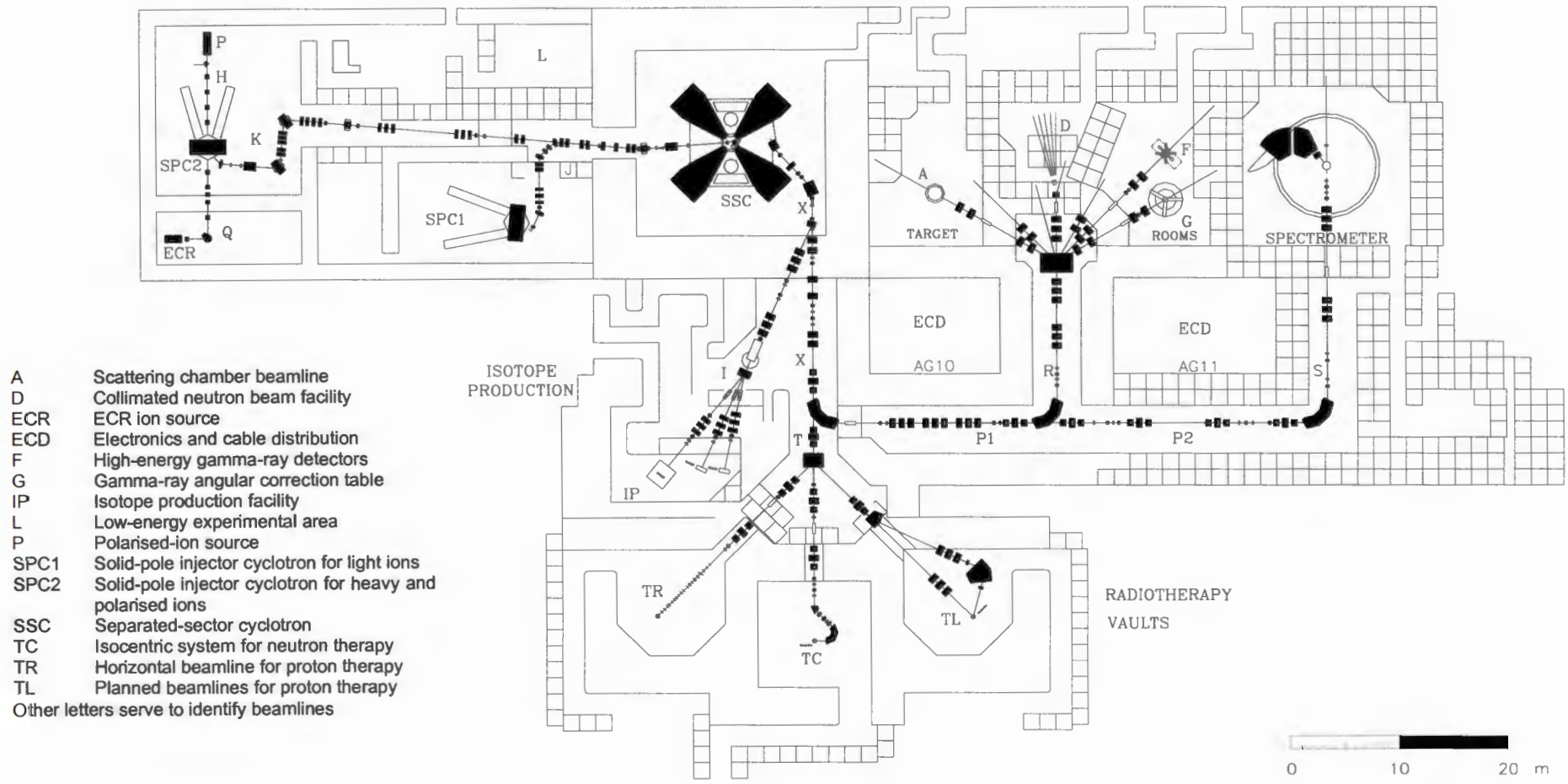

A	Scattering chamber beamline
D	Collimated neutron beam facility
ECR	ECR ion source
ECD	Electronics and cable distribution
F	High-energy gamma-ray detectors
G	Gamma-ray angular correction table
IP	Isotope production facility
L	Low-energy experimental area
P	Polarised-ion source
SPC1	Solid-pole injector cyclotron for light ions
SPC2	Solid-pole injector cyclotron for heavy and polarised ions
SSC	Separated-sector cyclotron
TC	Isocentric system for neutron therapy
TR	Horizontal beamline for proton therapy
TL	Planned beamlines for proton therapy

Other letters serve to identify beamlines

Fig.2.1: Layout of the iThemba LABS cyclotron facilities.

2.3 THE ACCELERATORS

2.3.1 THE 6 MV VAN DE GRAAFF ACCELERATOR

The 6 MV Van de Graaff accelerator **[NAC76]** is a high-precision, variable-energy machine, capable of accelerating light and light heavy ions to energies of between 0.5 and 20 MeV. The iThemba LABS Van de Graaff accelerator, which is in operation since 1962, is used mainly for materials and solid-state physics research in collaboration with the universities and technikons, as well as with local and international laboratories.

The layout of the Van de Graaff beamlines is shown in figure 2.2. The main facilities at the Van de Graaff accelerator are for atomic and solid-state physics and the application of nuclear analytical techniques in ion beam analysis and materials sciences. Research projects use accelerated particles for identification and quantification of elements in microelectronics, archaeology, geology, superconducting materials, optical layers and new materials. The high-brightness scanning nuclear microprobe, which has a resolution of less than 1 micron **[NAC76]**, enables the researchers to observe, identify and measure precise quantities of trace elements, as well as more abundant elements, in samples from many different fields.

Facilities for target manufacture, surface preparation and radioactivity counting are available. Radioactive tracers and nuclear techniques are utilised in basic and applied investigations. Data acquisition and analysis are fully computerised.

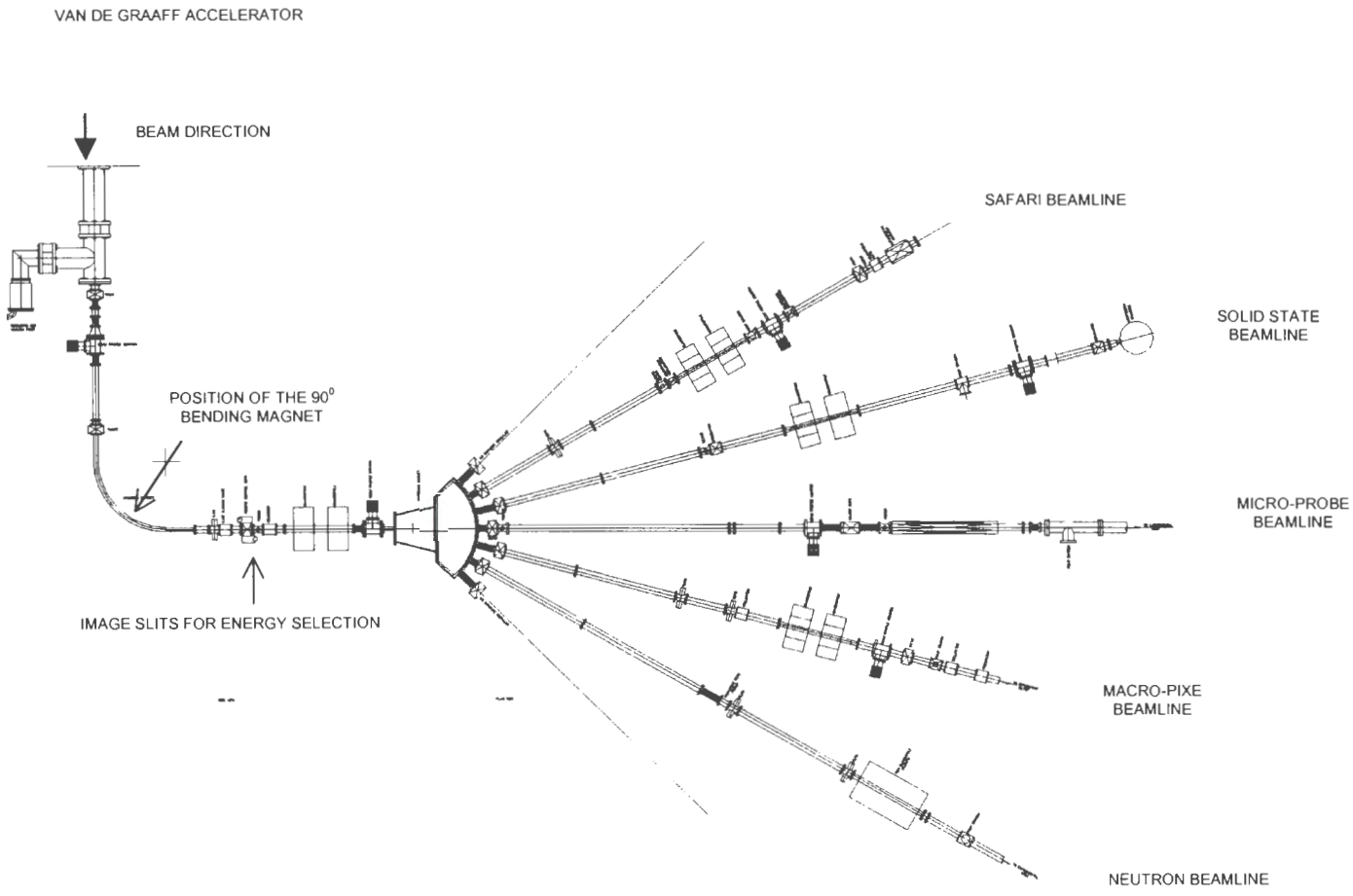

Fig.2.2: Layout of the existing beamlines at the Van de Graaff accelerator.

2.3.2 THE LIGHT-ION SOLID-POLE INJECTOR CYCLOTRON (SPC1)

The layout of SPC1 is shown in figure 2.3. It pre-accelerates and provides beams of light ions, especially protons, which can be injected into the SSC for further acceleration. SPC1 uses an internal PIG ion source to produce the intense beams of protons required for protontherapy, neutrontherapy and radioisotope production. This four-sector cyclotron, with four radial magnet sectors, has an extraction radius of 0.476 m, at which the beam is extracted with an electrostatic channel and two magnetic channels. The quarter-wave resonators, connected to 90^0 dees, and driven by two 20 kW power amplifiers, are used for acceleration on harmonic numbers 2 and 6 (see appendix A). Dee voltages of up to 60 kV and three constant orbit geometries are required to accommodate the desired particle and energy ranges **[NAC76, CON92, DUT87]**. Feedback systems stabilize the amplitude and phase of the dee voltage in order to obtain stabile beams.

2.3.3 THE SECOND SOLID-POLE INJECTOR CYCLOTRON (SPC2)

SPC2, which has a K-value of 10 for heavy ions, pre-accelerates and provides beams of both heavy ions (such as Carbon, Krypton, Titanium and Xenon) and polarised hydrogen ions (e.g. proton and deuteron beams) for the SSC, from its two external ion sources, i.e. a polarised ion source and an ECR ion source. SPC2 is in many respects similar to SPC1 but uses axial injection from the two external ion sources.

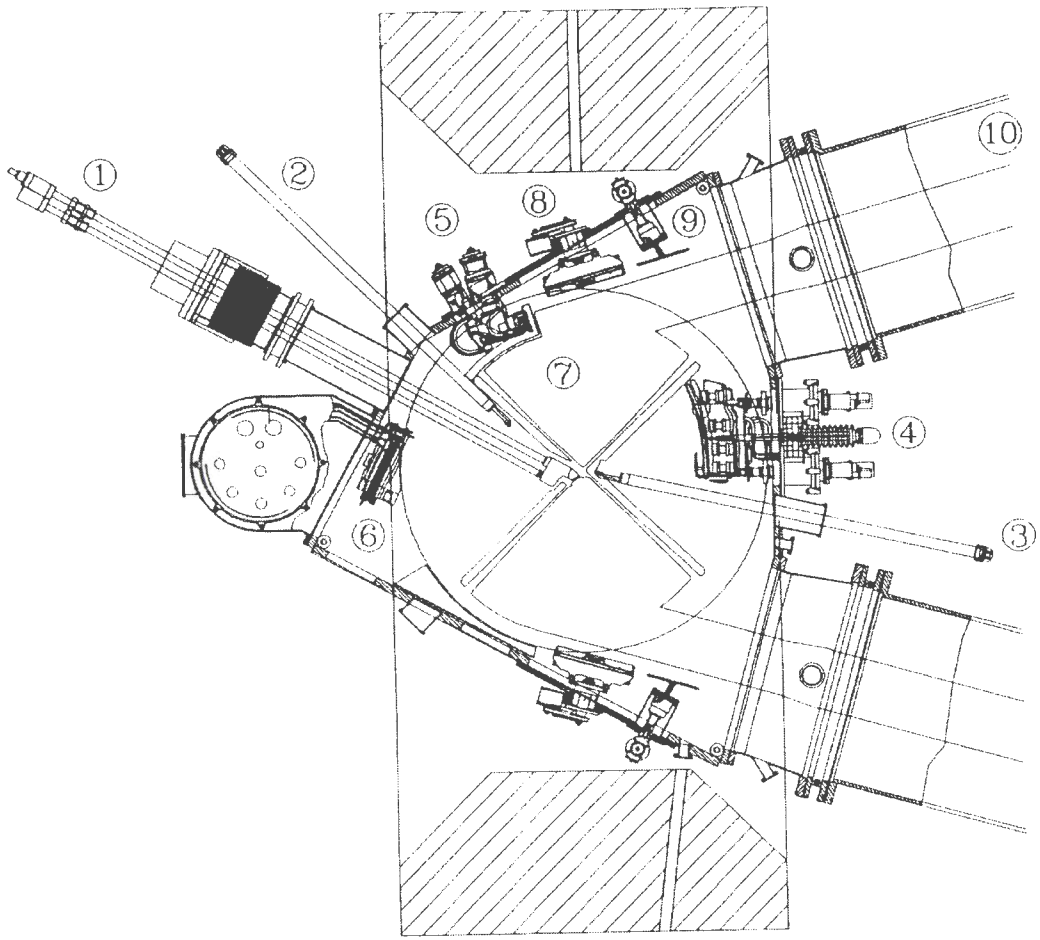

LEGEND

1. Ion source
2. ΣΔR probe 2
3. ΣΔR probe 1
4. Electrostatic extraction channel (EEC)
5. Magnetic extraction channel 1 (MEC 1)
6. MEC 2
7. A dee
8. Coupling capacitor
9. Trimming capacitor
10. A resonator

Fig.2.3: A median plane cross section through SPC1.

The layout of SPC2 is shown in figure 2.4. It is a solid-pole cyclotron with four radial magnet sectors. The beam is extracted with an electrostatic channel and two magnetic channels at a radius of 0.476 m. Beams from both the polarised ion source and an ECR source are injected axially from below into the cyclotron. Two quarter-wave resonators are used for acceleration (see appendix A) **[NAC76, CON92, BOT87]** and are driven by two 20 kW power amplifiers. Harmonic numbers 2 and 6 can be used for acceleration. Feedback systems stabilize the amplitude and phase of the dee voltage in order to obtain stable beams. The diagnostic equipment includes a harp, which can be positioned near the extraction radius for optimisation of the magnetic field.

2.3.4 THE SEPARATED-SECTOR CYCLOTRON (SSC)

The layout of the SSC is shown in figure 2.5. It is the main accelerator at iThemba LABS and has, for special purposes, accelerated protons to a maximum energy of 227 MeV. The SSC has a diameter of 13.2 meters and a height of 7 m. The four sector magnets are positioned to an accuracy of 0.1 millimetres and weigh about 1400 tons in total. The vacuum chambers are mounted in the pole gaps and in the two valleys. The magnet sector angle is 34^0 and the maximum flux density of 1.3 T occurs near the extraction radius for 200 MeV protons (see appendix A) **[NAC76, CON92]**.

The RF system consists of two half-wave resonators which can be tuned by means of movable short-circuit plates and adjustable capacitor plates in a frequency range of 6 to 26 MHz. The rf power of 85 kW per resonator is required to produce a dee voltage of 220 kV at 26 MHz. The injection system consists of two bending magnets, a magnetic inflection channel and an electrostatic channel. Extraction is accomplished with an electrostatic channel and two septum magnets **[NAC76, CON92]**.

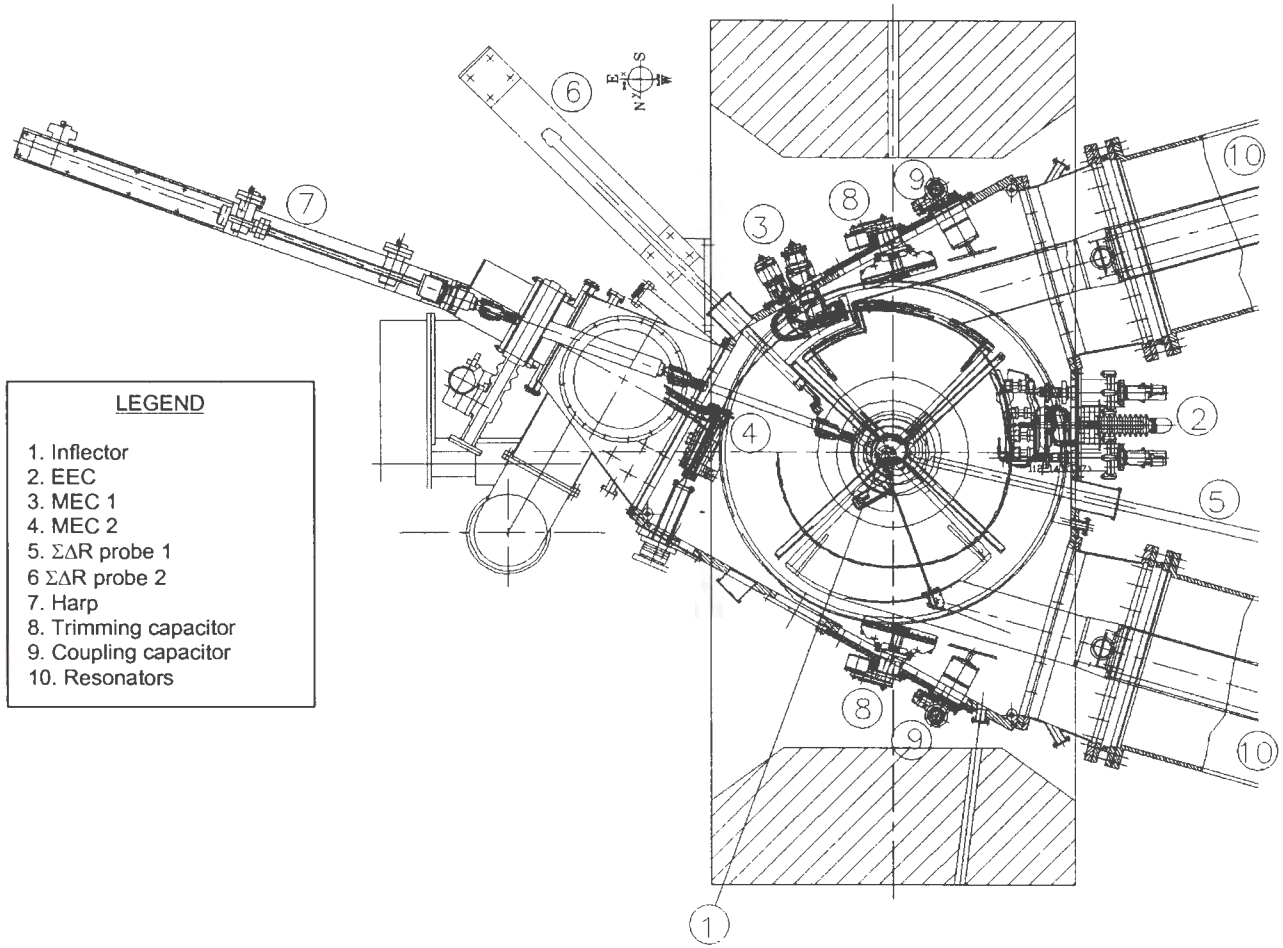

Fig.2.4: A median plane cross section through SPC2.

LEGEND

1. Injection Collimators
2. Harp
3. Beam Profile Scanner
4. Capacitive Phase Probe
5. Harp
6. MIC Collimators and Liners
7. Axial Graphite Collimators
8.& 9. Multi-head Probes
10. Beam Stop
11. Extraction Harp
12. Extraction Harp
13. Extraction Scanner
14. EEC-Collimators
15. SPM1-Collimators and Liners
16. SPM2-Collimators and Liners
17. Extraction Collimators
18. Electrostatic Inflection Channel Collimators
19. Radial Slit
20. Beam Centering Harp

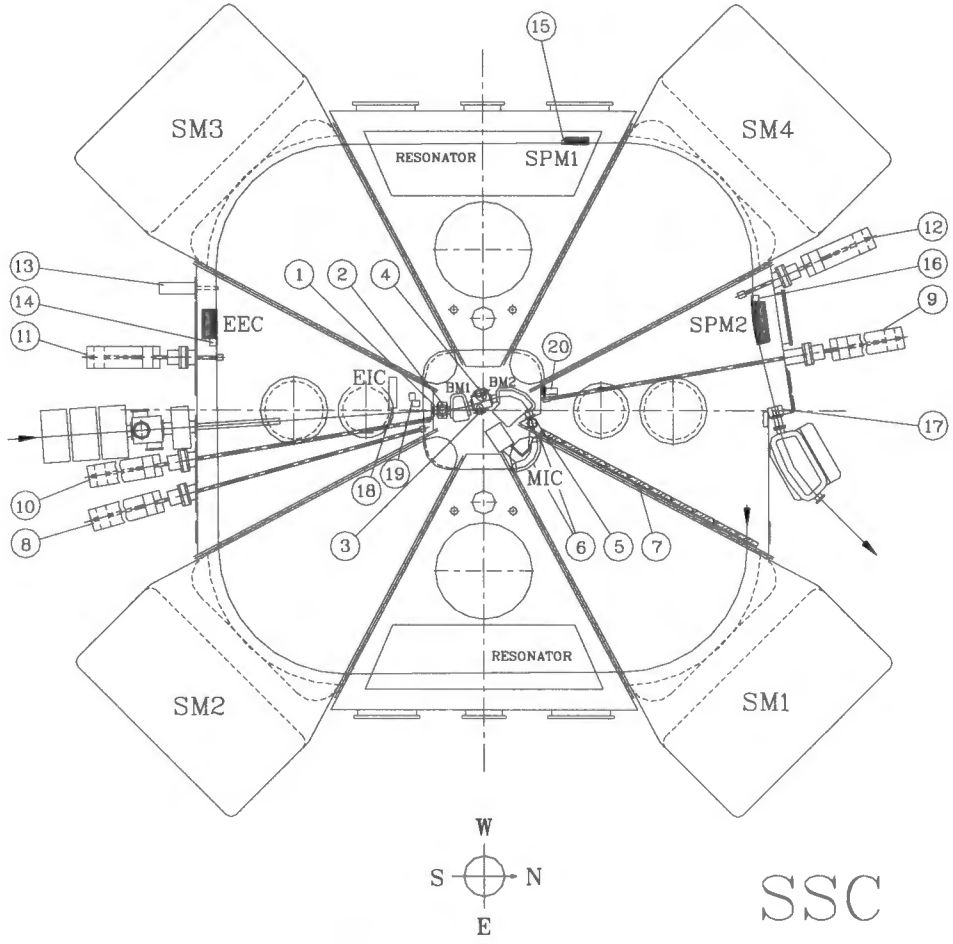

Fig.2.5: A median plane cross section through SSC.

CHAPTER 3

BEAM TRANSPORT FORMALISM

3.1 INTRODUCTION

Accelerated charged particle beams are transported through evacuated beam pipes. Because of the inherent divergence in the beam, provision has to be made for focussing of the beam. In general this is done with quadrupole magnets. Dipole magnets are employed for changes in the beam direction but can also be designed to contribute to the focussing of the beam.

For the design of beamlines, it is convenient to consider the behaviour of the beam in phase space in addition to the dimensions and position of the beam in laboratory space. For this purpose the computer program TRANSPORT **[CAR98]** is used in all major accelerator laboratories. This program calculates first-, second- and third-order effects by matrix multiplication. The beam optical elements and the charged particle beam are represented by matrices.

This general matrix evaluation and fitting program calculates or fits typical element values for the given beam conditions. It can evaluate various matrices that represent the transmission of particles through a beamline, and vary the physical parameters of the beamline to fit elements of such matrices to the desired values. These elements and conditions are specified by the user **[CAR98]**.

The program normally calculates the beam envelope and beam transfer matrices for the whole beamline using values for the physical parameters as specified by the user and prints the result. It has provision to vary some of the input parameters to achieve a desired final beam. A beamline envelope can be calculated and analysed.

The aim in designing a beamline is to compile a system of beamline elements such as quadrupole and dipole magnets that will transport the beam with the required characteristics to the users targets.

3.2 MATHEMATICAL FORMALISM OF TRANSPORT

An arbitrary charged particle at any specified position in a beamline may be represented by a six component vector, **X**, in co-ordinate form, in phase space. The components of this vector are the horizontal and vertical positions, the divergence in the horizontal and vertical planes, the path length difference between the particle and the central trajectory and the momentum spread. These co-ordinates are measured with respect to a specified reference trajectory that is taken to be the trajectory of the central particle of the ensemble of particles under consideration **[BRO77, MER80, CAR81]**.

The vector **X** describes the co-ordinates of a particle at a given position along the beamline and is made up as follows:

$$\mathbf{X} = \begin{bmatrix} x_1 \\ x_2 \\ x_3 \\ x_4 \\ x_5 \\ x_6 \end{bmatrix} = \begin{bmatrix} x \\ \theta \\ y \\ \phi \\ \ell \\ \delta \end{bmatrix} \qquad (3.1)$$

where:

- x is the horizontal displacement of the particle from the central axis of the beam,
- θ is the angle of the particle trajectory in the horizontal plane,
- y is the vertical displacement of the particle from the central axis of the beam,
- ϕ is the angle of the particle trajectory in the vertical plane,
- ℓ is the difference in the path length of the particle and that of the reference particle,
- δ is the fractional momentum deviation of the particle $\left(\Delta p / p\right)$ with respect to the reference particle.

To determine the vector **X** at any location (1) in the beamline from the vector at the initial position (0), the transfer matrix **R** of the beam elements in between can be used **[CAR81]**, such that,

$$X_1 = RX_0 \tag{3.2}$$

The elements of the 6x6-transfer matrix **R** for a beamline element are found by solving the equations of motion of a particle in the magnetic field of the element. **R** describes the effect of the beam transport element on the phase space co-ordinates of the particle. The total transfer matrix $\mathbf{R}_T$ then describes the effect of a system of elements, and can be determined from the product of the individual matrices $R_{(i)}$ as follows:

$$R_T = R_{(n)}R_{(n-1)}\ldots R_{(3)}R_{(2)}R_{(1)} \tag{3.3}$$

For static magnetic fields with midplane symmetry, **R** has several elements which are identically equal to zero and takes the form **[BRO77, BRO67]**:

$$R = \begin{bmatrix} R_{11} & R_{12} & 0 & 0 & 0 & R_{16} \\ R_{21} & R_{22} & 0 & 0 & 0 & R_{26} \\ 0 & 0 & R_{33} & R_{34} & 0 & 0 \\ 0 & 0 & R_{43} & R_{44} & 0 & 0 \\ R_{51} & R_{52} & 0 & 0 & 1 & R_{56} \\ 0 & 0 & 0 & 0 & 0 & 1 \end{bmatrix} \tag{3.4}$$

The zero elements R_{13}, R_{14}, R_{23}, R_{24}, R_{31}, R_{32}, R_{41}, R_{42}, R_{36} and R_{46} in the **R** matrix result from a midplane symmetry of the magnetic field. The zero elements R_{15}, R_{25}, R_{35}, R_{45} and R_{65} result from the fact that the variables x, θ, y, ϕ and δ are independent of the path length difference, because of the static magnetic field. The zeros of R_{61}, R_{62}, R_{63}, R_{64} and R_{65} are due to the fact that the momentum is a constant of motion and the field is time-independent. Whilst the zeros of R_{53} and R_{54} result from the fact that ℓ and the (y,ϕ) plane are decoupled **[MER80, BRO77, HEN74]**.

Because of the midplane symmetry, the co-ordinates (x,θ) and (y,ϕ) are always orthogonal. The other non-zero matrix elements can be explained by inspecting their dimensions **[DAV83]**, that is:

$R_{11} = \left(x_n / x_o \right)$
$R_{33} = \left(y_n / y_o \right)$ } transverse linear magnification

$R_{22} = \left(\theta_n / \theta_0 \right)$
$R_{44} = \left(\phi_n / \phi_0 \right)$ } angular magnification

$R_{21} = \left(\theta_n / x_0 \right)$
$R_{43} = \left(\phi_n / y_0 \right)$ } have dimensions of $\frac{1}{L}$ and is the inverse of the focal length

$R_{12} = \left(x_n / \theta_0 \right)$
$R_{34} = \left(y_n / \phi_0 \right)$ } have dimension of L and represent effective drift lengths through the system

$R_{16} = \left(x_n / \delta_0 \right)$ } d_x, the linear momentum dispersion

$R_{26} = \left(\theta_n / \delta_0 \right)$ } d_θ, the angular momentum dispersion

$R_{51} = \left(\ell / x_0 \right)$
$R_{52} = \left(\ell / \theta_0 \right)$ } terms mixing (x,θ) and (ℓ,δ) co-ordinate pairs in bending magnets

R_{56} – has dimensions of length and represent the effective length of a system for longitudinal co-ordinates

$R_{55} = 1$

$R_{66} = 1$

The transfer matrix **R** contains 36 elements of which 21 are equal to zero and therefore independent of the magnetic fields in beamline components.

Since we are dealing with static magnetic fields:

$$Det[R] = 1 \qquad (3.5)$$

Equation (3.5) holds for any element that does not change the momentum of the central trajectory. The determinant of any transformation matrix that describes the motion of particles in static magnetic fields has a value of +1 **[EMM63, BRO81, PEN61]**.

3.3 σ-MATRIX FORMALISM

We are, however, interested in the behaviour of a beam of particles rather than that of an individual particle. A multi-dimensional phase ellipse formalism is often used to represent such an aggregate of particles. Equation (3.2) can be extended further to encompass the behaviour of a bunch of particles as it passes through a transport system **[BRO77, CAR73]**. The equation of an n-dimensional ellipsoid in matrix form is,

$$X(0)^T \sigma(0)^{-1} X(0) = 1 \tag{3.6}$$

where $X(0)^T$ is the transpose of the co-ordinate vector X(0), and σ(0) is a real, positive definite, symmetric matrix.

As a particle passes through a system of beamline components such as drift spaces and quadrupole and dipole magnets, its behaviour in the six-dimensional space, defined above, is described by successive multiplication of the matrices for the individual beamline components with the vector **X**, according to the transformation given by equation (3.2). Combining this transformation with the equation of the initial ellipsoid (3.6), and using the identity matrix,

$$RR^{-1} = I \tag{3.7}$$

it follows that:

$$X(0)^T \left[R^T R^{T^{-1}}\right] \sigma(0)^{-1} \left[R^{-1} R\right] X(0) = 1 \tag{3.8}$$

from which we obtain:

$$\left[RX(0)\right]^T \left[R\sigma(0)R^T\right]^{-1} \left[RX(0)\right] = 1 \tag{3.9}$$

Then the equation of the new ellipsoid (representing the beam at the end of the system) after the transformation becomes:

$$X(1)^T \sigma(1)^{-1} X(1) = 1 \tag{3.10}$$

where the sigma matrix at the end is related to that at the beginning by:

$$\sigma(1) = R\sigma(0)R^T \tag{3.11}$$

Equation (3.11) is used by TRANSPORT to calculate the final beam from the initial. Equation (3.11) and (3.5) predicts equal determinants for $\sigma(1)$ and $\sigma(0)$. This implies equal phase space volumes for the two ellipsoids, and thus phase space volume is conserved under the transformation R. This is an expression of Liouville's theorem which states that the phase space volume occupied by a group of particles cannot change its size, although it generally will change its shape while traversing a beamline with static magnetic fields **[PEN61, KLA65, BRO77]**.

By calculating the product matrix, R, TRANSPORT computes the sigma matrix at the end of each physical element via equation (3.11). A beam ellipse in phase space is defined by the following symmetric sigma matrix:

$$\sigma = \begin{bmatrix} \sigma_{11} & \sigma_{21} \\ \sigma_{21} & \sigma_{22} \end{bmatrix} \tag{3.12}$$

The inverse of the matrix is given by;

$$\sigma^{-1} = \left(\frac{1}{\varepsilon^2}\right)\begin{bmatrix} \sigma_{22} & -\sigma_{21} \\ -\sigma_{21} & \sigma_{11} \end{bmatrix} \tag{3.13}$$

where ε^2 is the determinant of the sigma matrix.

For the 2-dimensional (x,θ) plane, the vector **X** and its transpose are:

$$X = \begin{bmatrix} x \\ \theta \end{bmatrix} \quad \text{and} \quad X^T = \begin{bmatrix} x & \theta \end{bmatrix} \tag{3.14}$$

The expansion of equation (3.10) (using equations (3.13) and (3.14)) gives the following equation for the ellipse in the (x,θ) plane:

$$\sigma_{22}x^2 - 2\sigma_{21}x\theta + \sigma_{11}\theta^2 = \varepsilon^2 = \det\sigma \tag{3.15}$$

Since this is the most general form of the equation for an ellipse centred about the origin the assumption of a symmetric matrix above is justified. The (x,θ) plane beam ellipse represented by equation (3.15) is shown in figure 3.1 along with the physical meaning of the sigma matrix elements. All the important physical parameters of the beam ellipse may be expressed as functions of the elements of the sigma matrix at different locations.

The square roots of the diagonal elements of the σ-matrix are the maximum beam extent along the axes of the ellipse, and in the more general case along the axes of the six-dimensional ellipsoid. In the two-dimensional case above the maximum spatial extent of the ellipse, i.e. the half-width of the beam, x_{max}, is given by square root of σ_{11}, whereas σ_{22} gives the maximum angular divergence of the beam, θ_{max}:

$$\left.\begin{aligned} \sqrt{\sigma_{11}} &= x_{\max} \\ \sqrt{\sigma_{22}} &= \theta_{\max} \end{aligned}\right\} \tag{3.16}$$

The off-diagonal term σ_{21} determine orientation of the ellipse in phase space, i.e. relative to the x and θ axes. The correlation between x and θ depends on this term. In general, the correlation coefficients, r_{ij}, are defined as:

$$r_{ij} = r_{ji} \equiv \frac{\sigma_{ij}}{\sqrt{\sigma_{ii}\sigma_{jj}}} \tag{3.17}$$

The area of the ellipse is given as;

$$\begin{aligned} A &= \pi(\det\sigma)^{1/2} \\ &= \pi\sqrt{\sigma_{11}\sigma_{22} - \sigma_{12}{}^2} \\ &= \pi\sqrt{\sigma_{11}\sigma_{22}\left(1 - r_{12}{}^2\right)} \\ &= \pi x_{\max}\theta_{\text{int}} \\ &= \pi x_{\text{int}}\theta_{\max} \end{aligned} \tag{3.18}$$

The area of the 2-dimensional ellipse occupied by the beam in phase space is called the beam emittance and is given by equation (3.18).

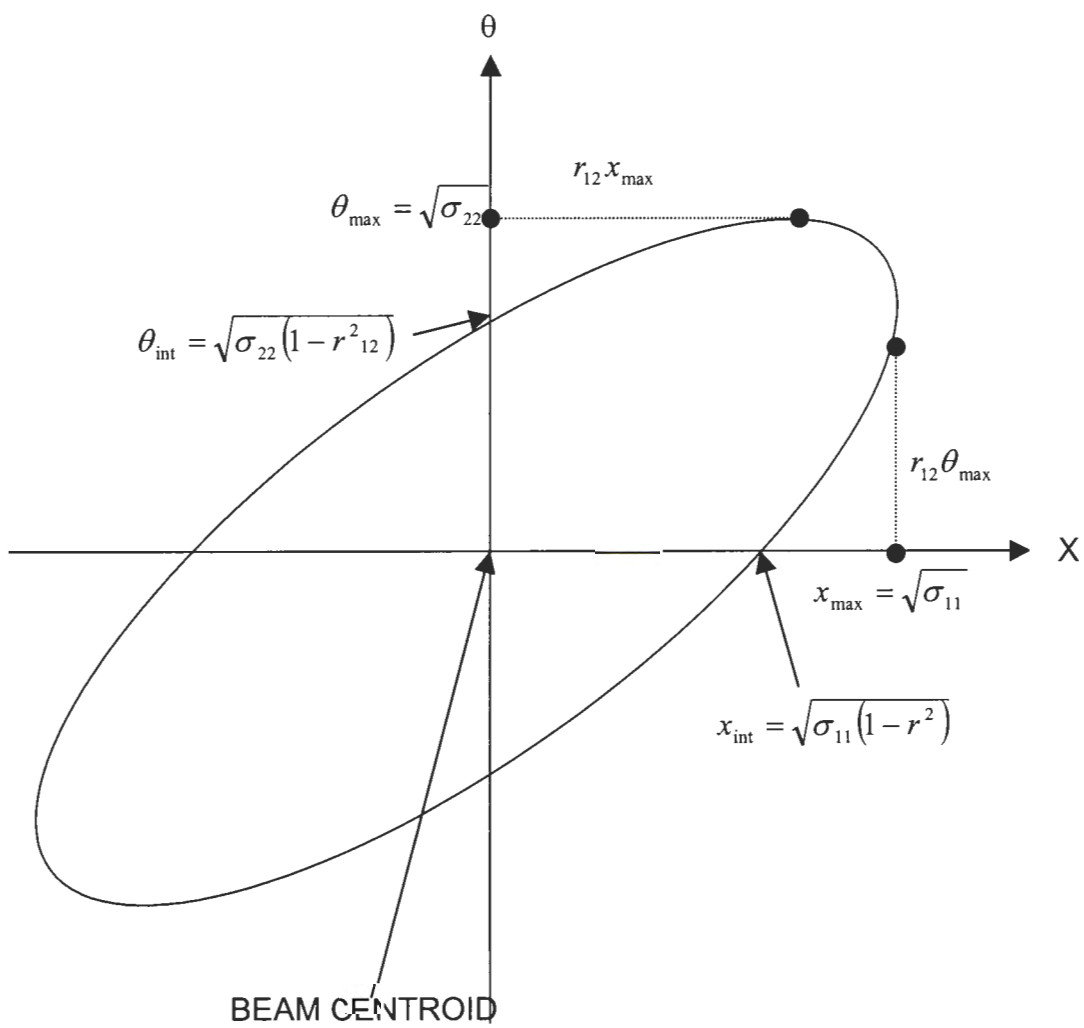

Fig.3.1: Important co-ordinates on a beam phase ellipse.

The matrix σ is used for the beamline design by the computer program TRANSPORT and is printed out in the format shown in table 3.1 **[CAR98, MER80]**.

TABLE 3.1: THE SIGMA MATRIX RESULTS FROM *TRANSPORT*.

			x	θ	y	ϕ	ℓ
x	$\sqrt{\sigma_{11}}$	cm					
θ	$\sqrt{\sigma_{22}}$	mr	r_{21}				
y	$\sqrt{\sigma_{33}}$	cm	r_{31}	r_{32}			
ϕ	$\sqrt{\sigma_{44}}$	mr	r_{41}	r_{42}	r_{43}		
ℓ	$\sqrt{\sigma_{55}}$	cm	r_{51}	r_{52}	r_{53}	r_{54}	
δ	$\sqrt{\sigma_{66}}$	%	r_{61}	r_{62}	r_{63}	r_{64}	r_{65}

The physical meaning of the $\sqrt{\sigma_{ii}}$ (i = 1 - 6) in table 3.1 being the maximum projection onto the six beam co-ordinates and gives the half-widths of the beam ellipsoid.

Other methods of beamline calculations, such as the method of 'Transfer Maps' that includes both the linear and non-linear beam elements **[DRA79]** and the lumped element and raytracing techniques incorporated in the computer programs TURTLE and RAYTRACE, respectively **[CAR72, SPE67]**, are also used in beamline design.

TURTLE (Trace Unlimited Rays Through Lumped Elements) is a Monte Carlo computer program used to simulate charged-particle beamline performance. It uses the same data format as in TRANSPORT and thus makes the switching from one to the other very easy. It allows the evaluation of the effect of aberrations (any deviation of the behaviour of a magnet system from the matrix analysis prediction) that exist in beams with small phase-space volumes **[PEN61, CAR81]**. The individual transformations through quadrupoles, sextupoles and solenoids are calculated by the program for each selected momentum value. The histograms and scatter plots of beam profiles and any intensity distribution or correlation can be produced. The second order terms and aperture constraints are also included in the calculations,

and the geometric effects on trajectories are limited up to the third order terms. The second order transformations for both the chromatic and geometric effects are used for a general bending magnet. The pole-face rotations with their accompanying fringe fields and the body of the bending magnet are all included in a single third-order transformation **[PEN61]**. The details and explanation on the pole-face rotation will be briefly described in the next chapter when dealing with the dipole magnet.

In spite of the availability of several calculation methods, the transfer matrix method is extensively used in beam transport design using the σ-beam matrix. In our case, the beamline will be designed from first order matrix calculations and also employing the σ-matrix.

CHAPTER 4

BEAM TRANSPORT ELEMENTS

4.1 INTRODUCTION

During the design of a beamline for the transport of charged particles, the characteristics of the transport elements, which are used to focus and direct the beam to the desired location, together with their matrix representations, have to be calculated. The calculations are iteratively repeated until the desired beam characteristics, as specified at the users' target or as specified for injection in a cyclotron, without any loss of beam along the beamline are obtained. A beam of charged particles that traverses a drift space, i.e. a field-free region, spreads out horizontally and vertically. Quadrupole and solenoid magnets are normally used to focus the beam. At low particle energies electrostatic quadrupoles can be used for focussing. Dipole magnets are employed to change the beam direction and bunchers are used for longitudinal focussing. The matrices of the beam elements that transport charged particles, i.e. drift spaces, quadrupole magnets, solenoids and dipole magnets, are explained below.

4.2 DRIFT SPACES

A drift length or space is a field-free region in the beamline through which the beam passes and is specified by a single parameter, L, its length. The co-ordinates of a particle after traversing a drift space are given in terms of the length of the drift space and the co-ordinates at the entrance to the drift space:

$$x_f = x_i + L\theta_i \text{, and } y_f = y_i + L\phi_i \tag{4.1}$$

where,

- x_f is the final particle displacement in the x-direction,
- y_f the final displacement in the y-direction,
- x_i the initial displacement in the x-direction,

y_i the initial displacement in the y-direction,

θ_i the initial angular divergence in the x-direction and

ϕ_i the initial angular divergence in the y-direction.

For six-dimensional phase space the first-order transfer matrix for a drift space is as follows **[CAR98]**:

$$R = \begin{bmatrix} 1 & L & 0 & 0 & 0 & 0 \\ 0 & 1 & 0 & 0 & 0 & 0 \\ 0 & 0 & 1 & L & 0 & 0 \\ 0 & 0 & 0 & 1 & 0 & 0 \\ 0 & 0 & 0 & 0 & 1 & \frac{L}{\gamma^2} \\ 0 & 0 & 0 & 0 & 0 & 1 \end{bmatrix} \tag{4.2}$$

where

L is the length of the drift space,

$\frac{1}{\gamma^2} = 1 - \frac{v^2}{c^2}$,

v the speed of the particles and

c the speed of light in vacuum.

4.3 QUADRUPOLE MAGNETS

When transporting a beam of charged particles, quadrupole magnets are normally used to keep the cross section of the beam from spreading out inordinately **[LIV69]**. A quadrupole provides focusing of the beam in one transverse plane and defocusing in the other and its focal strength can be computed from the magnetic field strength, aperture and length. Figure 4.1 shows the magnetic field lines of a quadrupole magnet with hyperbolic poles. A quadrupole with this pole configuration is termed positive for a beam travelling into the paper **[MER80]**. The first-order (positive) quadrupole transfer matrix is given by equation (4.3) **[CAR98]**:

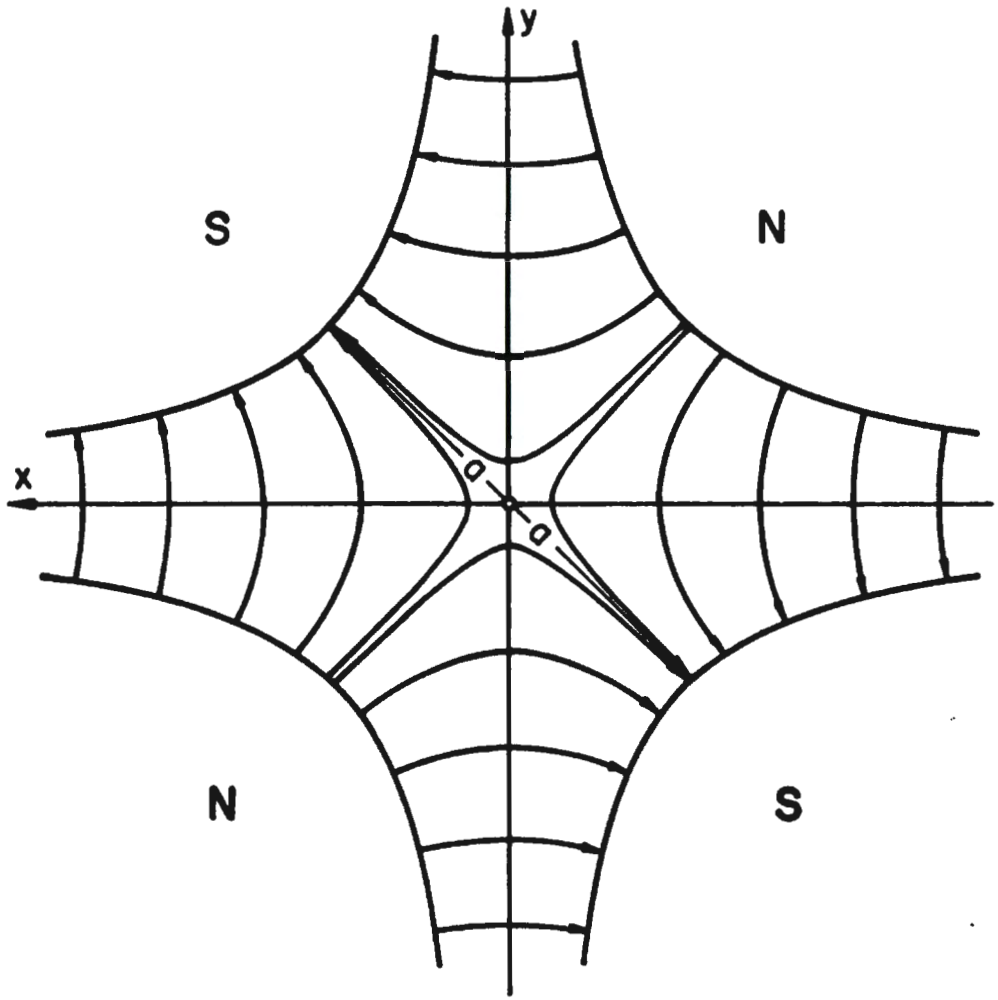

Figure 4.1: The direction of the magnetic field lines in a cross-sectional view of a quadrupole magnet with hyperbolic pole surfaces **[MER80]**.

$$R = \begin{bmatrix} \cos kL & \frac{1}{k}\sin kL & 0 & 0 & 0 & 0 \\ -k\sin kL & \cos kL & 0 & 0 & 0 & 0 \\ 0 & 0 & \cosh kL & \frac{1}{k}\sinh kL & 0 & 0 \\ 0 & 0 & k\sinh kL & \cosh kL & 0 & 0 \\ 0 & 0 & 0 & 0 & 1 & \frac{L}{\gamma^2} \\ 0 & 0 & 0 & 0 & 0 & 1 \end{bmatrix} \tag{4.3}$$

where

L is the effective magnetic length of the quadrupole,

$$k^2 = \frac{B_0}{a}\left(\frac{1}{B\rho_0}\right) \tag{4.4}$$

and a the radius of aperture of the quadrupole,

B_0 the magnetic field at the pole tip and

$B\rho_0$ the magnetic rigidity of the particle.

This matrix, R, presents the effect on a particle from the input face to the exit face of the quadrupole. The elements in the matrix above represent a quadrupole that focuses in the horizontal plane and defocuses in the vertical plane.

4.4 DIPOLE MAGNETS

The first order transfer matrix for a dipole magnet is given by equation (4.5) **[CAR98]**:

$$
R = \begin{bmatrix}
\cos k_x L & \frac{1}{k_x}\sin k_x L & 0 & 0 & 0 & \frac{1}{\rho k_x^{\,2}}\left(1-\cos k_x L\right) \\
-k_x \sin k_x L & \cos k_x L & 0 & 0 & 0 & \frac{1}{\rho}\sin k_x L \\
0 & 0 & \cos k_y L & \frac{1}{k_y}\sin k_y L & 0 & 0 \\
0 & 0 & -k_y \sin k_y L & \cos k_y L & 0 & 0 \\
-\frac{1}{\rho}\sin k_x L & -\frac{1}{\rho k_x^{\,2}}\left(1-\cos k_x L\right) & 0 & 0 & 1 & -\frac{1}{\rho^2 k_x^{\,3}}\left(k_x L-\sin k_x L\right)+\frac{L}{\gamma^2} \\
0 & 0 & 0 & 0 & 0 & 1
\end{bmatrix} \qquad (4.5)
$$

where, $k_x^{\,2} = \frac{1-n}{\rho^2}$,

$$k_y^{\,2} = nh^2, \tag{4.6}$$

ρ is the radius of curvature of the central trajectory,

L the path length of the central orbit,

n the normalized gradient of the bending magnet (dimensionless),

h the curvature of the central trajectory and

γ the relativistic factor.

This transfer matrix transforms the six co-ordinates of each particle in the beam that passes through the bending magnet from its entrance to the exit. Figure 4.2 shows the magnetic field boundaries of a dipole, bending magnet. Where R_1 and R_2 are the radii of curvature of the entrance and exit faces of the bending magnet, respectively.

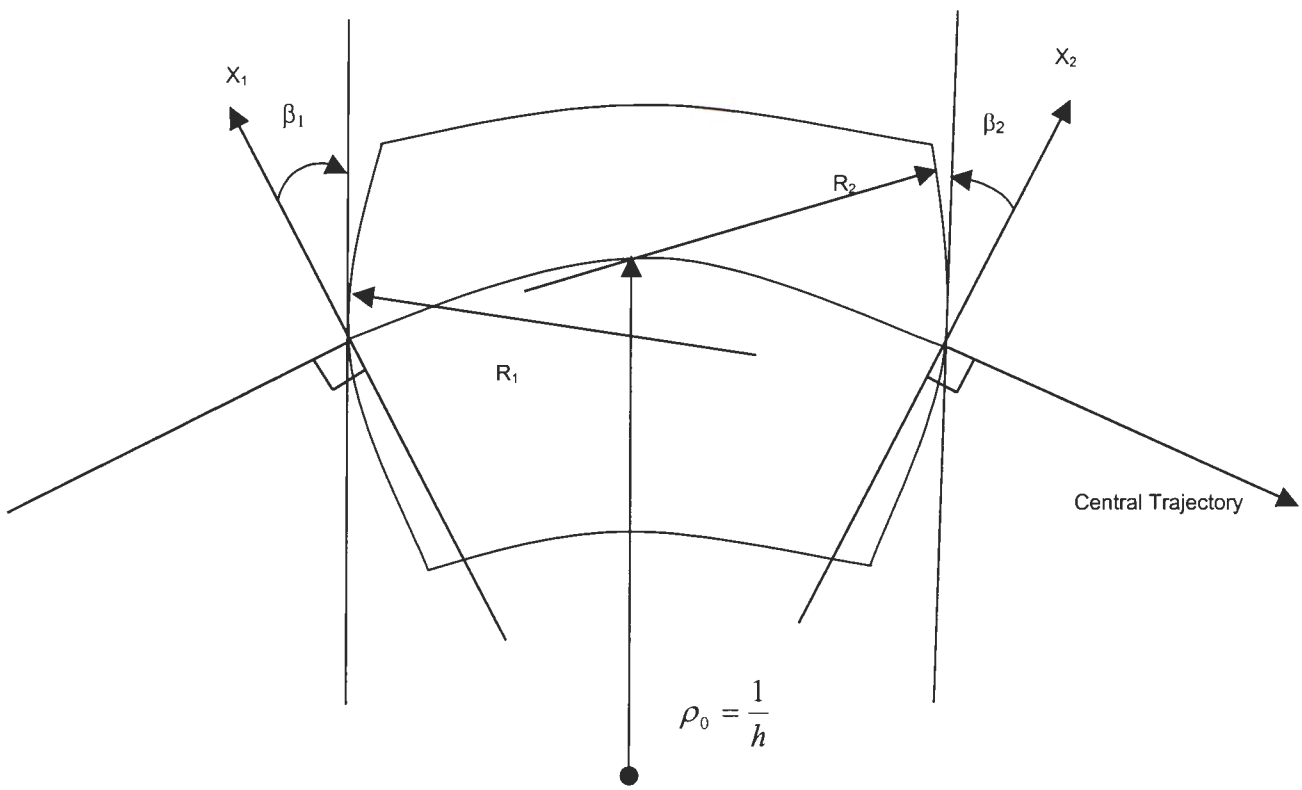

Fig.4.2: Magnetic field boundaries of a bending magnet and the entrance, β_1, and exit, β_2, pole face rotation angles of the beam.

The pole faces are the surfaces of the magnet that face the incoming beam (entrance pole face) and the beam where it leaves the magnet (exit pole face). Both the entrance and exit pole face rotation angles are used with bending magnets. The pole face rotation angle describes the deviation of the normal vector for a given pole face with respect to the incident or exit reference trajectory direction. The pole face rotation angles can be used to adjust the magnetic field path integral for the off-axis particles, in order to achieve different focusing conditions for those particles. The sign conventions for x, β, R and h, as shown in the figure 4.2, are all positive. The positive y direction is out of the paper. Positive β-values imply transverse focusing. Positive R-values (convex curvature) of the magnet edge introduce negative sextupole components of strength $S = \left(-h/2R\right)\sec^3\beta$ **[CAR98]**.

The first order transfer matrix for a pole-face rotation of edge-angle β, shown in figure 4.2, as used in a TRANSPORT calculation is **[CAR98, CHA98]**:

$$R = \begin{bmatrix} 1 & 0 & 0 & 0 & 0 & 0 \\ \frac{\tan\beta}{\rho_0} & 1 & 0 & 0 & 0 & 0 \\ 0 & 0 & 1 & 0 & 0 & 0 \\ 0 & 0 & -\frac{\tan(\beta-\psi)}{\rho_0} & 1 & 0 & 0 \\ 0 & 0 & 0 & 0 & 1 & 0 \\ 0 & 0 & 0 & 0 & 0 & 1 \end{bmatrix} \qquad (4.7)$$

where,

ρ_0 is the radius of curvature of the central orbit,

β the angle of rotation of the pole-face and

ψ a correction term resulting from the finite extent of the fringing fields.

4.5 SOLENOIDS

Solenoids are often used as focusing elements for a beamline that transports low-energy particles, i.e. of several tens of kilo-electron volts. Particles in a solenoidal field travel along the magnetic field lines with helical trajectories. The solenoid transformation is also used in conjunction with particle detectors in the interaction regions of particle colliders.

The first-order solenoid transfer matrix is given as follows **[CAR98]**:

$$R = \begin{bmatrix} C^2 & \frac{1}{K}SC & SC & \frac{1}{K}S^2 & 0 & 0 \\ -KSC & C^2 & -KS^2 & SC & 0 & 0 \\ -SC & -\frac{1}{K}S^2 & C^2 & \frac{1}{K}SC & 0 & 0 \\ KS^2 & -SC & -KSC & C^2 & 0 & 0 \\ 0 & 0 & 0 & 0 & 1 & \frac{L}{\gamma^2} \\ 0 & 0 & 0 & 0 & 0 & 1 \end{bmatrix} \quad (4.8)$$

where,

L is the effective length of the solenoid,

$K = \frac{B_0}{2B\rho_0}$, where B_0 is the field inside the solenoid and ($B\rho_0$) is the magnetic rigidity of the central trajectory,

C = cos KL,

S = sin KL,

$\frac{1}{\gamma^2} = 1 - \frac{v^2}{c^2}$, with v the speed of the particles and c the speed of light in vacuum.

4.6 BUNCHERS

Bunchers are used for focusing the beam longitudinally. To achieve the shortening of the pulse length along the beamline, the energy of lagging particles is increased and the energy of leading particles decreased by acceleration in a high frequency electrical field. The energy of the central particle in the beam remains unchanged whilst traversing the buncher and down-stream from the buncher the leading and lagging particles move closer to the central particle, which amounts to beam bunching.

The transfer matrix in longitudinal phase space is given by **[MER80]**:

$$\begin{bmatrix} R_{55} & R_{56} \\ R_{65} & R_{66} \end{bmatrix} = \begin{bmatrix} 1 & 0 \\ -1/f_b & 1 \end{bmatrix} \tag{4.9}$$

The focal length of the buncher, f_b, is half the focal length of each gap in a Klystron buncher **[CHA98]**, i.e.

$$f_b = \frac{1}{2}\frac{V_0 v}{V_{\max}\omega} \tag{4.10}$$

where,

- V_0 is the electric rigidity of the particles,
- V_{max} the amplitude of the sinusoidally varying voltage,
- v the speed of the particle and
- ω the angular frequency.

By approximating the sine wave with a linear relationship of voltage with time over a limited phase region the following expression relates the amplitude of a varying voltage and the electric rigidity;

$$V(l) \approx V_{\max}\omega\frac{l}{v} \tag{4.11}$$

where l is the length of particle bunch.

CHAPTER 5

DESIGN OF THE BEAMLINE BETWEEN AN EXTERNAL DUOPLASMATRON ION SOURCE AND SPC2

5.1 INTRODUCTION

In addition to the existing two external ion sources, i.e. the polarized ion source and the ECR ion source, a third ion source, for acceleration of high intensity beams of protons, is being planned for SPC2. With a suitable source for high intensity proton beams SPC2 could be used for the production of radioisotope and neutron-therapy when SPC1 is not in operation. Because of its low cost and simple construction a compact duoplasmatron ion source has been developed and will be evaluated for this purpose. In case this source does not meet the requirements in terms of intensity and beam quality a multi-cusp ion source, which is considerably more expensive and complicated to construct, will be considered.

The new source, which will also be external to SPC2, has to inject a beam into one of the existing injection beamlines of SPC2. A short new beamline is required to match the beam from the new source to the existing lines and SPC2. The computer program TRANSPORT will be utilized extensively for the design and optimization of this beamline, using measured beam emittance values of the duoplasmatron ion source. The new beamline should focus the beam from the duoplasmatron ion source to the horizontal and vertical focal conditions required at the first turn in SPC2.

5.2 THE INJECTION BEAMLINES OF SPC2

Figure 5.1 shows the layout of the existing ECR and polarized ion sources and their beamlines in a side view.

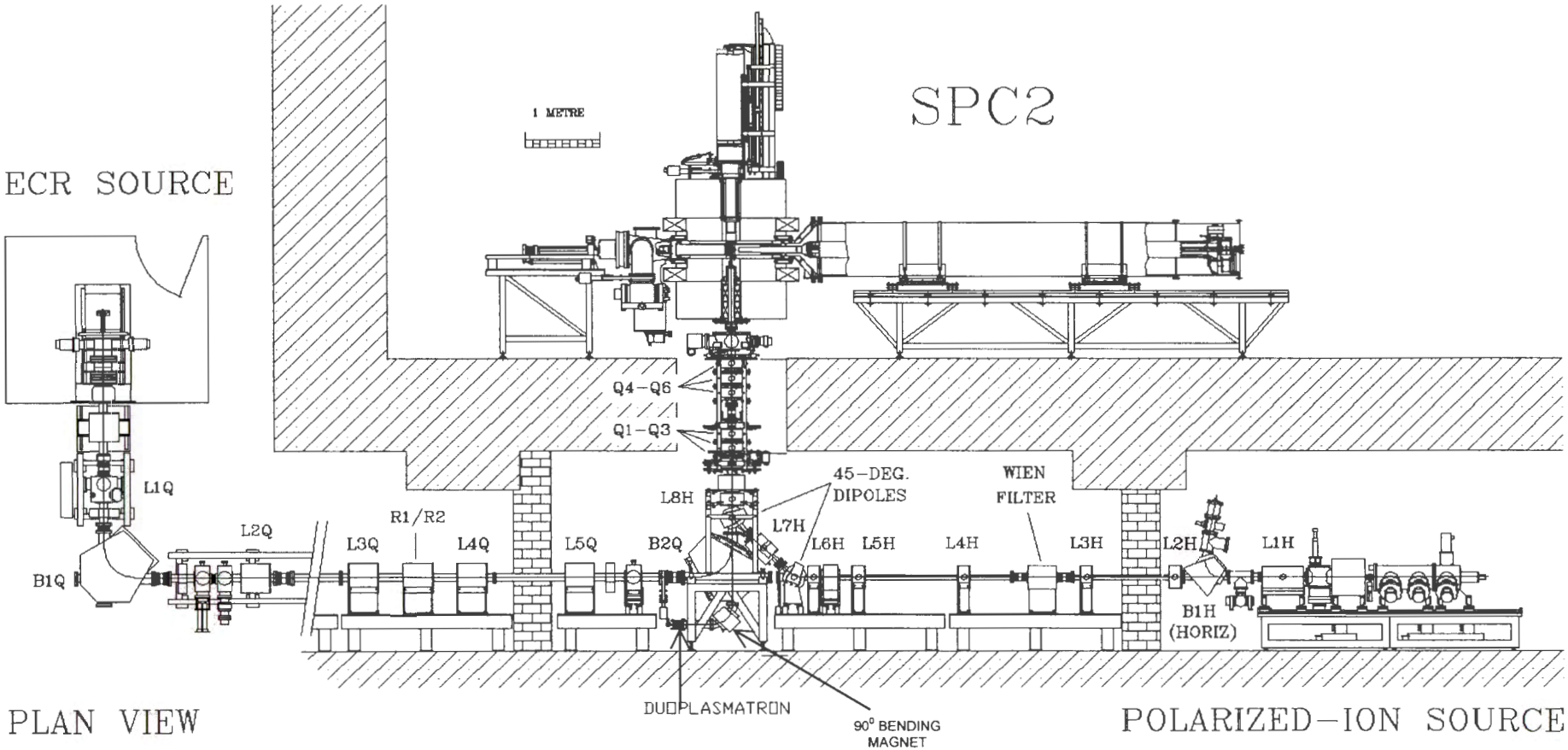

Fig.5.1: Layout of the injector cyclotron SPC2 and the existing ECR and Polarised Ion Sources with the planned position of the new Duoplasmatron Ion Source.

Solenoid L1Q focuses the beam in front of bending magnet B1Q, which is used for charge-state selection. Focusing of the beam from B1Q to B2Q is done by solenoids L2Q, L3Q, L4Q and L5Q. A particle beam from the ECR ion source is directed with two bending magnets B1Q and B2Q along the Q- and AX-beamlines to SPC2. Further beamline elements, quadrupoles Q1-Q6 and solenoids in the yoke of SPC2, are used for transporting and focusing of the beam in the center of SPC2. The proton beam from the polarized ion source is transported and focused with solenoids L1H to L8H and is bend by two 45^0 dipole magnets from the H-beamline into the AX-line, where it is then focused in SPC2.

The planned positions of the duoplasmatron ion source and the 90^0 bending magnet that will direct the beam into the H- and AX-beamlines, are indicated on the figure directly below the cyclotron. When this source is used the second 45^0 bending magnet at the intersection of the H- and AX-beamlines, will be switched off. With the new 90^0 bending magnet the beam will be focused in both the horizontal and vertical directions near the solenoid L8H.

5.3 THE BEAM EMITTANCE OF THE DUOPLASMATRON ION SOURCE

The beam extracted from the ion source has, in addition to its height and width, angular divergence in the horizontal and vertical directions. These, and other, beam properties are, as discussed in chapter 3, best described in six-dimensional phase space with the following coordinate axes, of which the particle on the beam axis, i.e. the central particle, defines the origin: the horizontal and vertical positional and angular deviations of particles as well as the longitudinal positional and energy deviations from the central particle. Instead of using the full six-dimensional phase space, if is often sufficient to consider the projections of the beam in the three phase planes formed by the following combinations of axes of the six-dimensional phase space: the horizontal positional and angular deviations, the vertical positional and angular deviations and the energy and longitudinal positional deviations. The regions occupied by beams in these phase planes are typically elliptical in shape. Various definitions of emittance, all related, exist. Emittance is for the present purpose defined as the area of the beam ellipse in a phase plane. The emittance in the horizontal and vertical directions has the units mm mrad and the factor π, used in the calculation of the area of the ellipse, is written explicitly to avoid confusion.

Determination of the emittance of the duoplasmatron ion source formed a part of another project **[MOK02]** and is therefore not discussed here. The following values have been obtained for 86% of the beam at an extraction energy of 16 keV using the double slit method:

Beam emittance in the vertical direction: 270 π mm mrad
Beam emittance in the horizontal direction: 270 π mm mrad

Transformed to an extraction voltage of 20 kV these values become 234 π mm mrad that will further be used for the design of the new beamline components and for determining the required settings of existing beamline elements.

5.4 DESIGN OF THE NEW BEAMLINE

In order to focus the beam from the source with solenoid L8H and the existing components in the AX-beamline, the beam should have a double waist, i.e. the beam should be focused in both directions, at a distance of 400 mm in front of L8H. The required width of the waist depends on the beam emittance. In principle the source could be installed at this position but the presence of the second 45^0 bending magnet does not permit this. Furthermore the source does not deliver a pure beam of protons only. Unwanted ions, mainly charged hydrogen molecules, have to be removed from the beam before injection into SPC2, where components can be damaged due to overheating when these unwanted particles collide with them. The best way to separate the molecular ions from the protons is with a bending magnet of sufficiently large bending radius and a slit. Because of the difference in momentum of protons and molecular hydrogen ions with the same energy, the radii of curvature in the field of the bending magnet also differ. Ions with different masses are therefore spatially separated by the bending magnet and unwanted particles can be removed by an appropriate positioning of the jaws of a slit, but allow protons to pass through the slit. The planned bending magnet between the duoplasmatron ion source and the existing injection beamlines is indicated in figure 5.1. In order to satisfy the mentioned focusing requirements, the magnet will have to be designed as a double focusing beamline element with suitable entrance and exit edge angles to provide adequate focusing in both the horizontal and vertical directions, unless additional components such as solenoids and quadrupole magnets are used. Due to space limitations the latter option has not been considered.

Figure 5.2 shows calculated beam envelopes, using the program TRANSPORT, from the ion source through the 90^0 bending magnet and AX-beamline up to the centre of SPC2 for a beam emittance of 200 π mm mrad in both directions. The required beam waists along the beamline have been specified in the program TRANSPORT, which then varied the field strengths and gradients of the beamline magnets, the edge angles of the bending magnet and the ion source position in order to obtain beam transmission through the beamline. The optimum entrance and exit edge angles, for focusing in both the horizontal and vertical directions, are 28^0 and 23^0, respectively. Due to a large emittance of the source it was difficult to obtain conditions for which the beam would pass through the existing beamline and the source could therefore not be positioned at the image position of the double focusing bending magnet as would be preferred. In figure 5.2 the source is 300 mm closer to the bending magnet than the image position. The TRANSPORT input files used for the design of the beamline is given in Appendix B. The "T" and inverted "T" characters in figure 5.2 indicate the specified beam waists. Beam envelops for an emittance of 50 π mm mrad in both the horizontal and vertical directions are shown in figure 5.3.

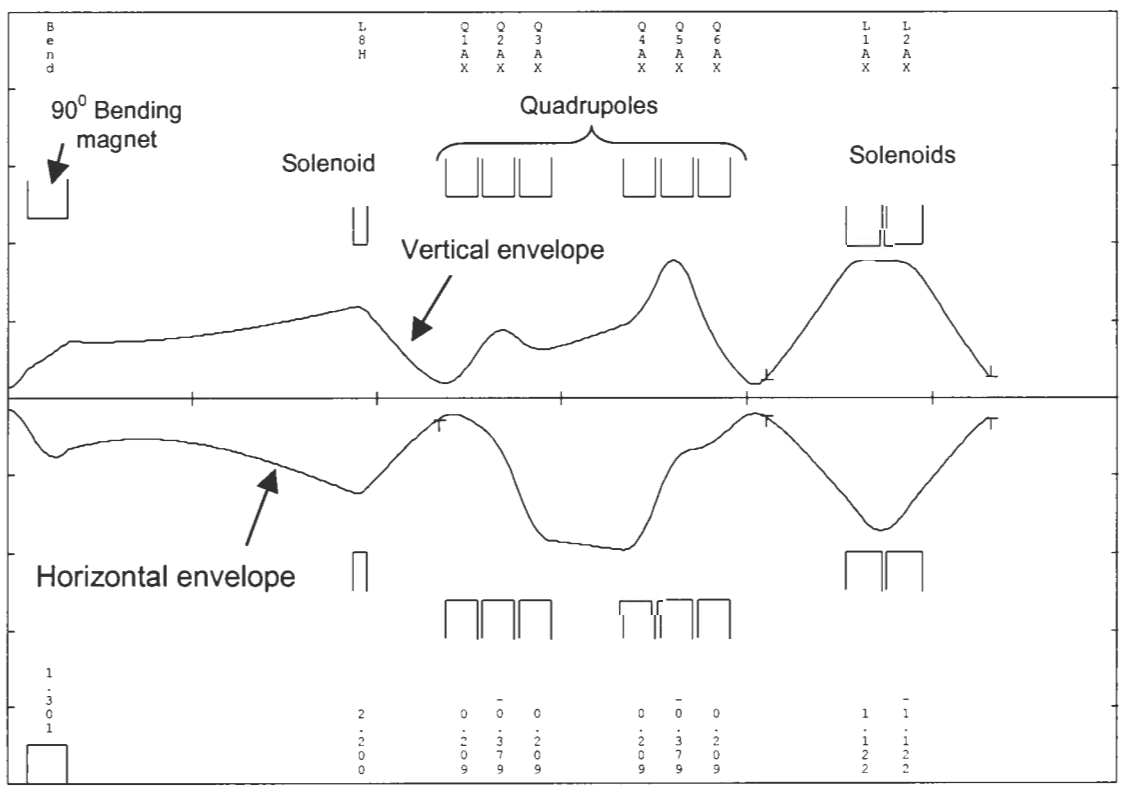

Fig.5.2: Calculated beam profiles in the beamline between the duoplasmatron ion source and SPC2 for an emittance of 200 π mm mrad in both directions.

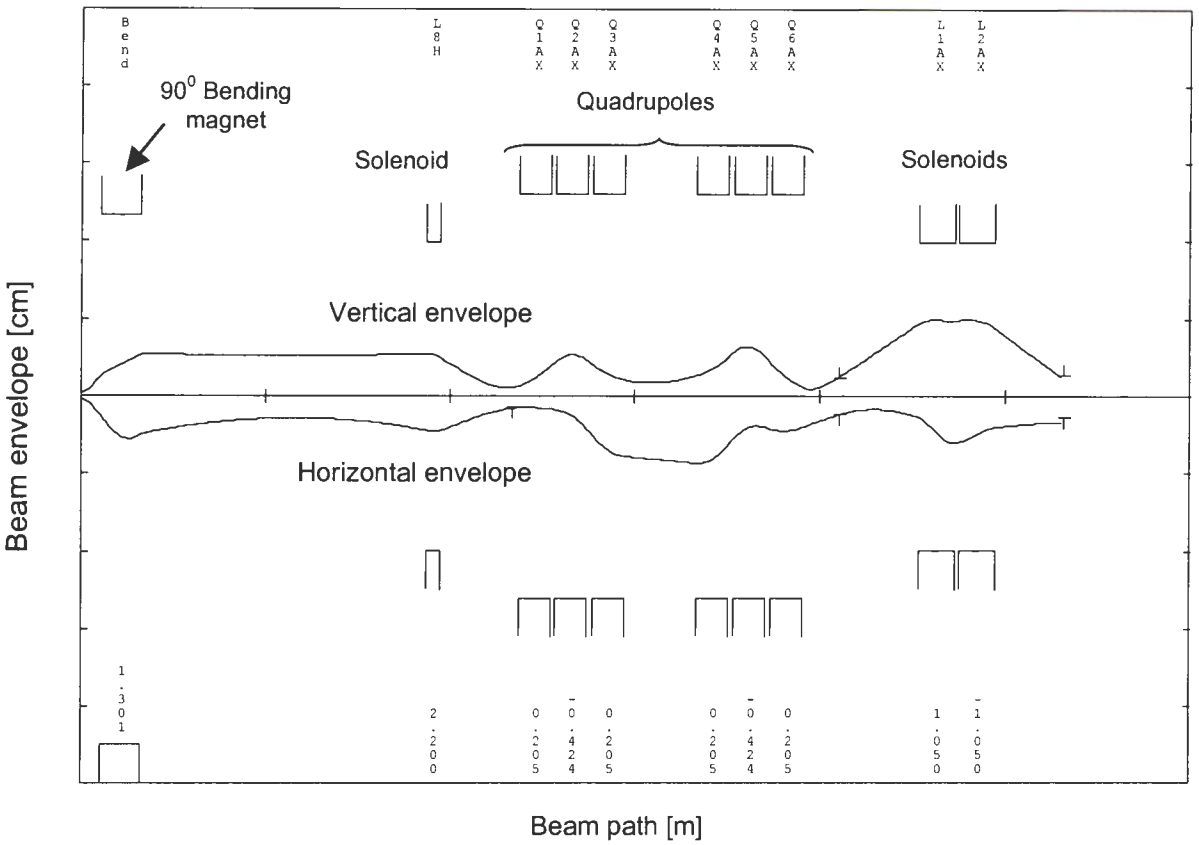

Fig.5.3: Calculated beam profiles in the beamline between the duoplasmatron ion source and SPC2 for an emittance of 50 π mm mrad in both directions.

5.5 CONCLUSIONS

A suitable position for coupling a third external ion source for high-intensity proton beams to the existing injection beamlines of SPC2 has been found. A double focusing 90^0 bending magnet for separation of the proton beam from unwanted molecular hydrogen ions has to be inserted between the source and the existing beamlines. To meet the required focal conditions the bending magnet has to focus the beam in both the horizontal and vertical directions. By calculation, using the program TRANSPORT, the best position for the ion source with respect to the magnet has been determined. Satisfactory beam envelopes could be obtained with the existing beamline elements up to the centre of SPC2. The field strengths of solenoid L8H and the beamline elements in the AX-beamline required for operation with the duoplasmatron ion source have been calculated. The detailed design of the 90^0 bending magnet will be discussed in the next chapter.

CHAPTER 6

DESIGN OF THE 90^0 BENDING MAGNET FOR THE BEAMLINE FROM THE DUOPLASMATRON ION SOURCE TO SPC2

6.1 INTRODUCTION

It is imperative that only protons are allowed to proceed from the duoplasmatron ion source to the SPC2 and to have the unwanted H_2^+ and H_3^+ ions removed from the beam as soon as possible after emerging from the ion source. A dipole magnet is therefore planned as a bending and analysing magnet very close to the extraction side of the duoplasmatron ion source. This configuration will ensure that most of the unwanted ions are separated from the protons. This will reduce the generation of heat and prevent damage to the injection and extraction components of SPC2 and also to the beam pipe leading to SPC2. The usual problems with space-charge effects will also be reduced with a proton beam only.

This dipole bending magnet will be designed from first principles approximation using analytical expressions for its most important characteristics and then further optimised by using the computer program Opera-3d with the TOSCA module for 3-dimensional finite-element numerical field analysis **[WWW1]**.

Aspects that will be discussed are the design parameters of the magnet, analytical expressions used for the design of an electromagnet, the analysing power of the magnet, the use of numerical field analysis computer codes for magnet design and characteristics of the magnet and its magnetic field.

6.2 DESIGN OF THE BENDING MAGNET FOR BEAM ANALYSIS

6.2.1 DETERMINATION OF THE BENDING ANGLE, BENDING RADIUS AND POLE GAP OF THE BENDING MAGNET

With the selection of the analysing magnet the following factors should be considered:

1. The particle energy and the required charge states resolving power of the magnet
2. The bending angle
3. The double focusing distance
4. The bending radius
5. Second order effects of the magnet
6. Dispersion caused by the magnet
7. The dimensions of the beam in the magnet

The above-mentioned factors are inter-dependent. For example, for a bending magnet with acceptable bending radius, double-focusing distance and analysing power, the second order effects could be unacceptable. For practical reasons due to the available space for incorporation of the duoplasmatron ion source in the existing layout, a 90^0 analysing magnet will be best suited. With the bending angle of the analysing magnet fixed a decision on the bending radius, double-focusing distance and the pole gap has to be made. These three variables are interlinked and must be treated simultaneously. The double-focusing distance, L_f, for a bending magnet with a bending angle, α, and bending radius, ρ, is given by **[NAC76]**:

$$L_f = 2\rho \cot\frac{\alpha}{2} \qquad (6.1)$$

Expression (6.1) describes a system that focuses in both the x and y directions at the same distance, L_f, from the magnet. For $\alpha = 90^0$, dictated by the layout of the injection beamline of SPC2, the distance L_f is given by:

$$L_f = 2\rho \tag{6.2}$$

For high charge states, mass and energy resolution a bending magnet with a large radius is needed (see equations 6.17 and 6.18), and a large radius implies a large double-focusing distance according to equation (6.2). The double-focusing distance influences the minimum required pole-gap of the magnet, for transmission of the beam. With the beam focused on the double-focusing distance of the magnet the minimum pole gap is given by:

$$\begin{aligned} g &\approx 2\dot{y}L_f, \\ &= \frac{2E_y L_f}{y\pi}, \end{aligned} \tag{6.3}$$

where,

g is the smallest allowable pole gap,

$\dot{y}$ the divergence of beam in y-direction $= \frac{E_y}{y\pi}$,

E_y the beam emittance in the y-direction and

y the half-width of the beam at the double-focussing point.

The maximum double focusing distance of a bending magnet with a pole gap of 70 mm, required for transmission of a beam with an emittance of 200 π mm mrad and a half width of 3 mm at the focus point, the required focal width for injection into SPC2 with this emittance, is:

$$\begin{aligned} L_f &= \frac{gy\pi}{2E_y}, \\ &= \frac{70 \times 3 \times \pi}{2 \times 200 \times 10^{-3} \times \pi}, \\ &= 525mm. \end{aligned}$$

A bending magnet with double focusing distance of 525 mm or smaller and a minimum pole opening of 70 mm is therefore acceptable. From previous calculations

[NAC76] and discussions the following characteristics is recommended for the analysing magnet:

Bending angle (α) = 90^0,
Bending radius (ρ) = 220 mm,
Pole gap (g) = 70 mm.

The maximum flux density variation across the beam region, Δx, inside an H-magnet can be restricted by choosing an appropriate pole width **[PAR76, CON85]**, e.g. for variations of 1% and 0.1% the respective required pole widths will be:

$$\Delta x_{0.01} \cong w - g\,, \tag{6.4}$$

$$\Delta x_{0.001} \cong w - 2g\,, \tag{6.5}$$

where *w* is the pole width and *g* is the pole gap.

Assuming a cross-sectional beam width of about 40 mm inside the magnet and less than 1% magnetic flux variation in the beam region, the minimum width of the pole must be (using (6.4)):

$$\begin{aligned} w &= g + \Delta x_{0.01}\,, \\ &= 70mm + 40mm\,, \\ &= 110mm\,. \end{aligned}$$

6.2.2 BASIC EQUATIONS USED FOR DESIGNING A BENDING MAGNET

For a particle with charge *q*, mass *m* and speed *v* moving perpendicular to a uniform, time-independent magnetic field, B, on a circular orbit with radius of curvature, ρ, the Lorentz force is equal to the centrifugal force:

$$qvB = \frac{mv^2}{\rho}\,,$$

$$\rho = \frac{mv}{qB}\,. \tag{6.6}$$

From expression (6.6) follows that the momentum, mv, can, for a given charge q, be expressed as the product of $qB\rho$. The product $B\rho$ is called the magnetic rigidity of the particle and is directly proportional to the particle's momentum **[GOL50]**. The expression relating the total energy E and the momentum p of a particle is:

$$E^2 = p^2c^2 + {m_0}^2c^2 \tag{6.7}$$

with m_0 the rest mass of the particle.

The magnetic rigidity is given by:

$$\begin{aligned} B\rho &= \frac{mv}{q}, \\ &= \frac{Ev}{qc^2}, \\ &= \frac{E}{qc}\beta \\ &= \frac{E}{qc}\frac{1}{\gamma}\sqrt{\gamma^2 - 1} \\ &= \frac{E}{qc}\frac{\sqrt{E^2 - {E_0}^2}}{E}, \\ &= \frac{\sqrt{{E^2}_k + 2E_0E_k}}{qc}. \end{aligned} \tag{6.8}$$

where,

$$\gamma = \frac{E}{E_0} = \frac{1}{\sqrt{1-\beta^2}},$$

$$\beta = \frac{v}{c},$$

c is the speed of light in vacuum,

v the velocity of the particle,

E_0 the rest energy of the particle,

q the charge of the particle and

E_k the kinetic energy of the particle.

The magnetic rigidity of 20 keV protons (the maximum energy for injection into SPC2) is:

$$B\rho = 0.0204Tm \tag{6.9}$$

This means that the radius of curvature in a field of 0.1 *T* is 204 *mm*. With the radius of the magnet known as required by the double focusing distance, the maximum field strength for the magnet can be calculated from (6.9) as:

$$B = \frac{0.0204Tm}{0.22m} = 0.0927T$$

If we assume that saturation will only be reached when the magnetic flux density in the iron is about 1.2 T, and that the flux that passes through the iron is the same as that which passes through the pole gap, the following calculation can be used to determine the minimum thickness of the iron yoke pieces.

Magnetic flux through the air (pole gap) = Magnetic flux through the iron

$$A_g \times B_g \cong y \times A_i \times B_i \tag{6.10}$$

where,

A_g is the area of the pole surface,

A_i the cross-sectional area of the yoke (= length x minimum width of a yoke piece)

B_g the magnetic flux density in the pole gap,

B_i the magnetic flux density in the yoke and

y the number of yoke pieces for closing of the magnetic flux loop, which is determined by the magnet shape (i.e. y=1 for a C-magnet and y=2 for an H-magnet).

The path-length, L, of a 90^0 circular bend is given by:

$$L = \frac{2\pi\rho}{4} = \frac{2\pi \times 220mm}{4} \approx 346mm\,.$$

Assuming an H-shape magnet, the minimum width of the yoke pieces can thus be calculated as follows:

$$\textit{Minimum width (yoke)} = \frac{A_g \times B_g}{2 \times B_i \times length(yoke)},$$

$$= \frac{346mm \times 110mm \times 0.0927T}{346mm \times 2 \times 1.2T},$$

$$= 4.3mm.$$

The yoke width was chosen as 20 mm because steel plates with such thickness were available. To create the magnetic field in the magnet a certain magnetomotive force (mmf) that will give the required flux density through the magnet has to be applied. The required mmf is generated by the coil windings of the magnet through which an electric current is send **[KRO68]**.

Following Ampere's law (the integral of the magnetic field along a closed path equals the enclosed total current):

$$\oint \vec{H} \cdot d\vec{l} = nI \qquad (6.11)$$

where,

H is the magnetic intensity or the field strength in A/m,

n the total number of turns in the windings and

I the current through a winding in A.

It is assumed that the magnetic flux density in the iron is the same as in the pole gap and that the direction of the field is parallel to the arrows of path a-b-c-d-e-g, as shown in figure 6.1. The field is calculated from the relation (6.11) such that;

$$H_g \times g + H_i \times l = nI \qquad (6.12)$$

where,

H_g is the magnetic intensity in the pole gap,

H_i the magnetic intensity in the iron,

l = a + b + c + d + e and

g pole-gap.

Substitute $l = 6g$ in expression (6.12) in order to obtain:

$$g\left(H_g + 6H_i\right) \cong Ni \tag{6.13}$$

The following equation gives the relationship between the magnetic flux density B and magnetic intensity H:

$$B = \mu_0 \mu_r H \tag{6.14}$$

where μ_r is the relative permeability of the material and

μ_0 the permeability of free space.

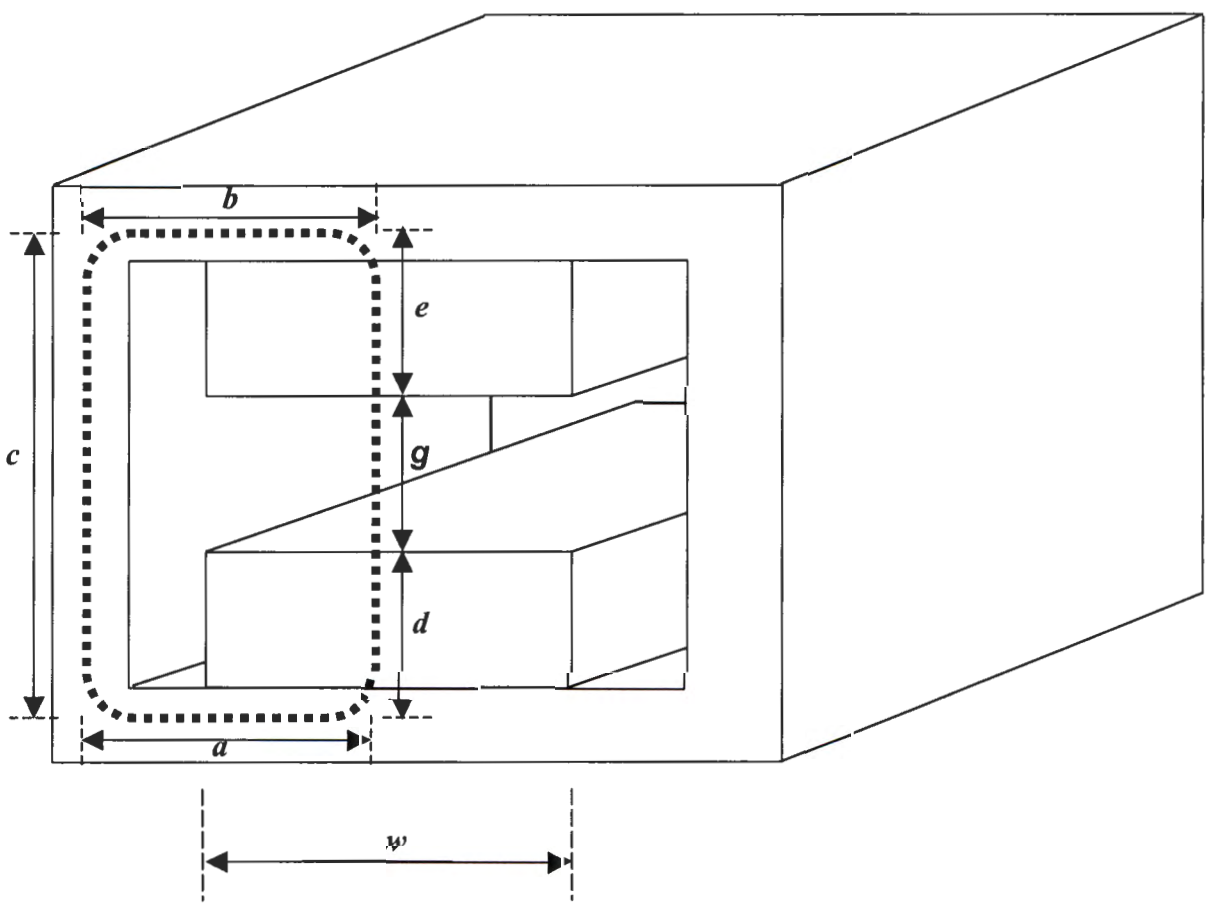

Fig.6.1: Schematic drawing of the integration path used to compute the field in the pole gap of an H-type dipole magnet, with a pole width w and pole gap g.

From equating equation (6.13) and (6.14), the following relation is obtained:

$$g\left(\frac{B_g}{\mu_0\mu_{air}}+\frac{6B_i}{\mu_0\mu_{iron}}\right)=nI \qquad (6.15)$$

The second term in relation (6.15) can be neglected for flux densities below 1.2 T. Hence the following approximation:

$$nI \approx \frac{gB_g}{\mu_0\mu_{air}} \qquad (6.16)$$

The required mmf to obtain a magnetic flux density of 0.0927 T in the air gap is then:

$$\begin{aligned} mmf &= nI \\ &= \frac{gB_g}{\mu_0\mu_{air}} \\ &= \frac{0.07m \times 0.0927T}{4\pi \times 10^{-7} Tm/A} \qquad (\mu_{air}=1) \\ &= 5164 \; ampere\text{-}turns \end{aligned}$$

The maximum tolerable current density for air-cooled coils is between 2 and 3 A/mm^2, depending on the coil geometry and we decided not to exceed 2 A/mm^2. The available copper wire with 2 *mm* diameter can thus carry a maximum current of 6.28 A. With the maximum current known the minimum number of windings for the required magnetic field can be calculated as:

$$n=\frac{mmf}{I}=\frac{5164}{6.28}\approx 822(turns)$$

A safety factor of 25% is added to the number of windings, hence the minimum total number of about 1027 windings for the coils. The four coils were built with 330 turns each (total of 1320 turns), using 2mm diameter copper wire and thus operating at a current of 4.35 A (a current density of 1.385 A/mm^2) to give the required magnetic

field in the pole gap. A rough estimate of the total length of the coils is 400 m. The resistance of the 400 m copper wire with thickness of 2 mm is:

$$R = \frac{l}{A_{wire}}\rho,$$

$$= \frac{400m \times 0.01754\Omega mm^2/m}{3.14mm^2},$$

$$\approx 2.23\Omega.$$

where,

l is the length of the coils in m,

ρ the resistivity of copper (= 0.01754 $\Omega\, mm^2/m$ at 25 ^{0}C) and

A_{wire} the cross-sectional area of the wire.

It has been decided on a wire with 2 mm diameter because it is readily available and will suit the geometry and available space.

The voltage required for the maximum current of 6 A is:

$$V = I \times R = 6A \times 2.23\Omega = 13.38V.$$

And the power consumption of the magnet is:

$$P = I \times V = 6A \times 13.38V = 80.28W.$$

6.3 ANALYZING POWER OF THE MAGNET IN TERMS OF ENERGY, MOMENTUM, CHARGE AND MASS

For the sake of simplicity of the equations, non-relativistic approximations for the momentum and kinetic energy will be used in this chapter since the velocity of a 20 keV proton is much smaller than the speed of light in vacuum. The relation between momentum, kinetic energy and charge state is thus derived from the following approximations, $E = \frac{1}{2} mv^2$, $p = mv$ and $\frac{1}{2} mv^2 = qU$,

where E is the kinetic energy of the particle,

m the mass of the particles,

q the charge of particles,

U the voltage difference between the source and the beamline,

p the momentum of the particles and

v the speed of the particles.

From the previous three equations follows:

$$\frac{dE}{E} = 2\frac{dp}{p} = \frac{dq}{q} \tag{6.17}$$

The resolving power of the magnet is defined as the momentum change $\Delta p/p$ that is required to shift the image of the object slit with the width of the image, namely:

$$\frac{\Delta p}{p} = \frac{2M_H x_0}{D\rho} = \frac{2R_{11}x_1}{R_{16}} \tag{6.18}$$

where D is the shift in the position of image per unit change in ρ,

ρ the radius of curvature of the central particle's orbit,

M_H the horizontal enlargement and

X_1 the half-width of the object slit.

R_{11} and R_{16} are matrix elements of the transfer matrix from the object slit to the image slit (the same notation as in the computer program TRANSPORT is used here).

Figure 6.2 shows the typically bending action of the bending magnet at different stages along the particle trajectory. Note that the numbers indicate the positions at which the matrix coefficients change in value. The object distance is S_1. Position 1 is at the object; 2 is just outside the entrance effective edge, and 3 is just inside it; 4 and 5 are similarly at the two sides of the effective exit edge and 6 is at any distance S_6 beyond the magnet. The elements R_{11} and R_{16} for a bending magnet with bending angle α and object slit and image slit as in figure 6.2 are given as calculated and described below **[LIV69]**.

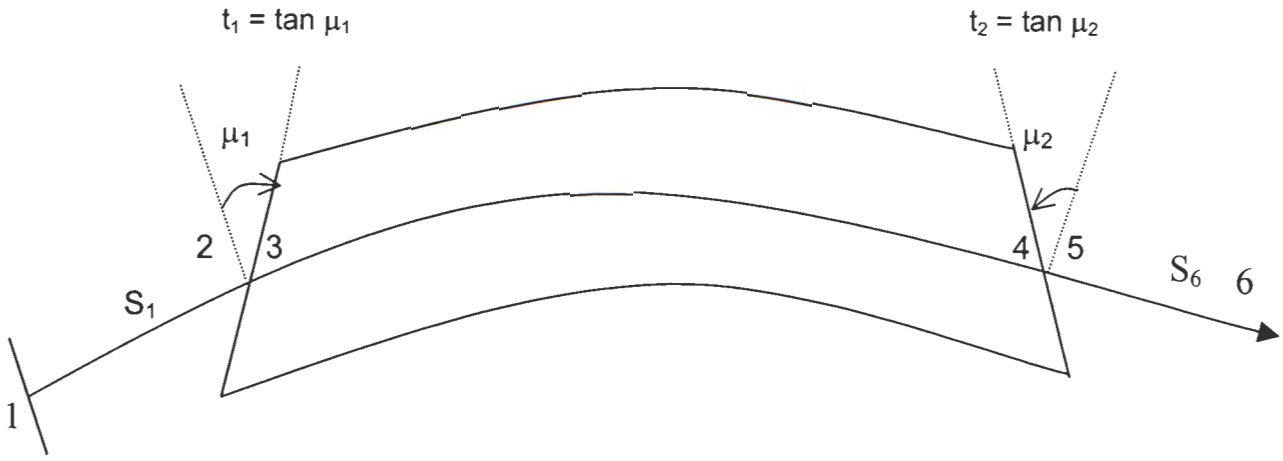

Fig.6.2: A schematic drawing of a particle track from the source object point, passing through a dipole magnet to the image point.

$$X_6 = R_{11}\, x_1 + R_{12}\, \dot{x}_1 + R_{16}\frac{dp}{p} \qquad (6.19)$$

$$R_{11} = -\{(S_1/\rho)[\sin\alpha - (t_1 + t_2)\cos\alpha - (t_1\, t_2 \sin\alpha)] - \cos\alpha - t_1 \sin\alpha\} \qquad (6.20)$$

$$R_{12} = \rho \sin\alpha + S_0[\cos\alpha + t_1 \sin\alpha] - S_1\, S_2\, (S_o/\rho)[\sin\alpha - (t_1 + t_2)\cos\alpha - (t_1\, t_2 \sin\alpha)] - \cos\alpha - t_2 \sin\alpha\} \qquad (6.21)$$

$$R_{16} = \rho\,(1 - \cos\alpha) + S_1\,[t_2\,(1 - \cos\alpha) + \sin\alpha] \qquad (6.22)$$

For the analysing magnet with a bending radius of 220 mm, edge angles of $29{,}8^0$ and double focusing distance of 525 mm (the edge angle and double focusing distance were determined with the TRANSPORT program), R_{11} is given by:

$$R_{11} = -\frac{44}{22}[\sin 90^0 - (2 \tan 29.8^0)\cos 90^0 - \tan 29.8^0 \sin 90^0] - \cos 90^0 - \tan 29.8^0 \sin 90^0\}$$

$$= 0.8350$$

$$R_{16} = 22\,(1 - \cos 90^0) + 44\,[\tan 29.8^0\,(1 - \cos 90^0) + \sin 90^0]$$

$$= 0.911 \text{ cm/\%}$$

For the values of R_{11} and R_{16} in equation (6.18), the momentum resolution of the bending magnet with a 10 mm object slit is equal to:

$$\frac{\Delta p}{p} = \frac{2R_{11}x_1}{R_{16}}$$

$$= \frac{2 \text{ x } 0.8350 \text{ x } 0.5}{0.911}$$

$$= 0.916\%$$

The energy resolution of the magnet is given by,

$$\frac{\Delta E}{E} = 2\frac{\Delta p}{p} = 1.832\%$$

and the charge state selection that can be done with the magnet is:

$$\frac{\Delta q}{q} = 2\frac{\Delta p}{p} \approx \frac{1}{5}$$

Particles that have different mass but the same energy will have different momenta. Since $E = \frac{1}{2}mv^2 = \frac{p^2}{2m}$ is fixed,

$$\frac{\Delta m}{m} = 2\frac{\Delta p}{p} = 1.832\%$$

The largest $\frac{m}{\Delta m}$ that can be resolved is called the 'mass resolution' and it is half of the 'momentum resolution'. The separation, Δx, of two masses after the magnet is equal to:

$$\Delta x = \frac{R_{16}}{2}\frac{\Delta m}{m} \approx 0.83cm$$

The object slit width cannot just be made smaller and smaller to achieve any desired resolution because beam intensity will be reduced, and the beam size at the image

slit will also become dominated by the second and higher order aberrations. The easiest way to achieve high resolution is by scaling the system larger, since R_{16} is directly proportional to the radius of the magnet, but at some point the cost of manufacturing a bending magnet with an excessively large radius, will become too big.

Due to the fact that the beam from the duoplasmatron ion source has a small energy spread it is not required to do energy selection with the magnet and it can separate charges very effectively with its 1:5 separation ratio.

6.4 CALCULATED MAGNET CHARACTERISTICS USING THE COMPUTER PROGAM *TOSCA*

Tosca is a computer program for 3-dimensional numerical field calculations using finite elements analysis and is a module of the OPERA-3d software package developed by the company Vector Fields. TOSCA has proven to be an innovative product in the finite element electromagnetic analysis techniques and is renowned for its accuracy of computation **[WWW1]**.

TOSCA is used for optimising the magnet geometry, edge angles and homogeneity of the magnetic field of the 90^0 bending magnet.

6.4.1 90^0 BENDING MAGNET GEOMETRY

The calculated finite element geometry of the H-shape bending magnet is shown in figure 6.3 with two sets of coils around the lower pole. The upper coils are omitted from the figure to reveal the geometry of the yoke, pole and pole plates with the field homogenizing shims. Three calculated trajectories are shown superimposed on the geometry, diverging horizontally from a source point in the median plane and then bend through 90 degrees (moving towards the viewer) and converge to the focal point.

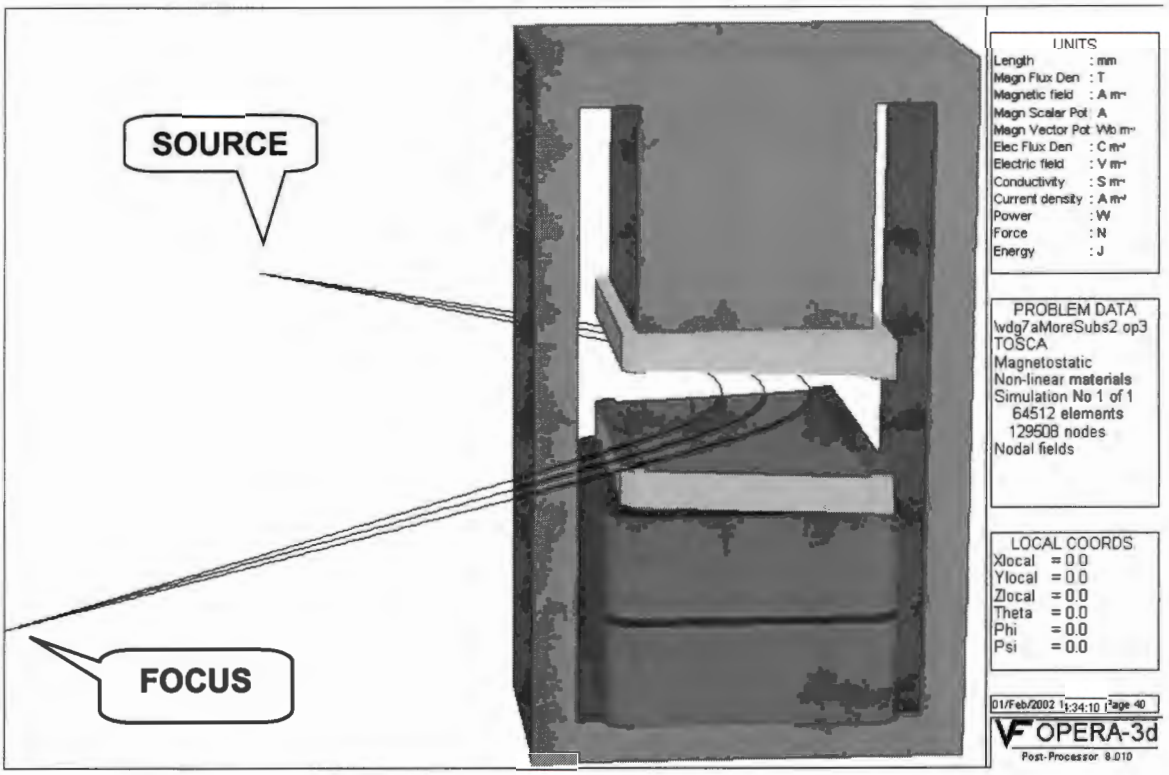

Figure 6.3: A perspective view of the magnet geometry with only the lower coils displayed, showing the shape of yoke, entrance and exit edges of the pole plates and side shims, with calculated beam trajectories superimposed on the geometry.

The edge angles of the pole plates were determined as shown in figure 6.4, to give the least difference in the horizontal and vertical focal lengths of calculated beam trajectories. Linear interpolation between the calculated focal lengths of two magnets with different edge angles resulted in an optimised minimum difference of focal lengths for a magnet edge angle of 34.7^0.

Calculation of a new magnet with an edge angle value of 34.7^0 confirmed the equal horizontal and vertical focal lengths expected from the linear interpolation. A magnet with an edge angle of 34.7^0 was manufactured.

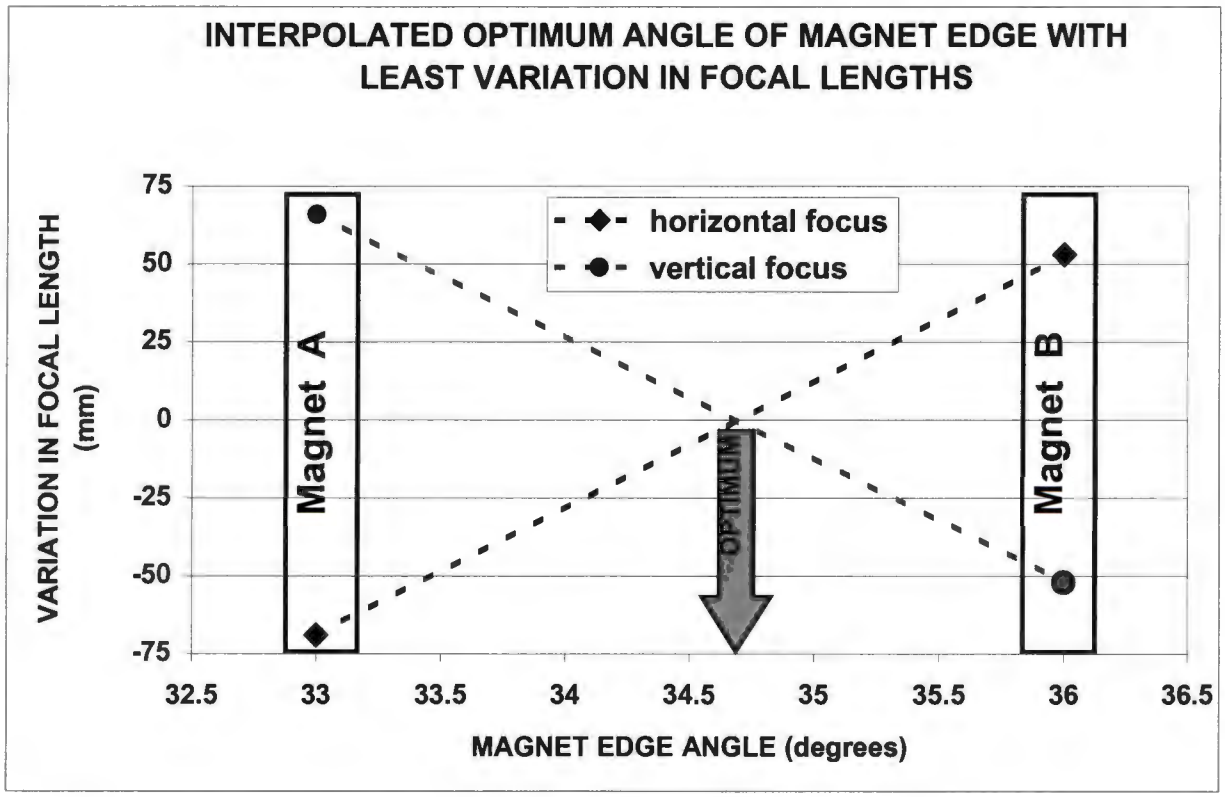

Figure 6.4: The optimum edge angle of 34.7^0 of the magnet was determined by linear interpolation of the respective calculated horizontal and vertical focal lengths of two magnets, A and B, with respective edge angles of 33^0 and 36^0.

6.4.2 MAGNETIC FIELD DISTRIBUTION

- **Excitation curve**

The excitation curve of the bending magnet was determined by both measurement and calculation. A maximum coil current of 10 A created a magnetic field of about 0.18 T. The higher excitations were applied for short periods only, to prevent overheating of the coils. If a high current (larger than 6 A) is to be applied additional cooling of the coils (e.g. cooling fans) must be implemented.

The relationship between the current and magnetic field values is graphically represented in figure 6.5, which shows the typical initial linear field increase, which then gradually proceeds towards saturation as the current increases. However, the magnet has negligible magnetic field saturation effects at the intended operational current value of 4.35 A.

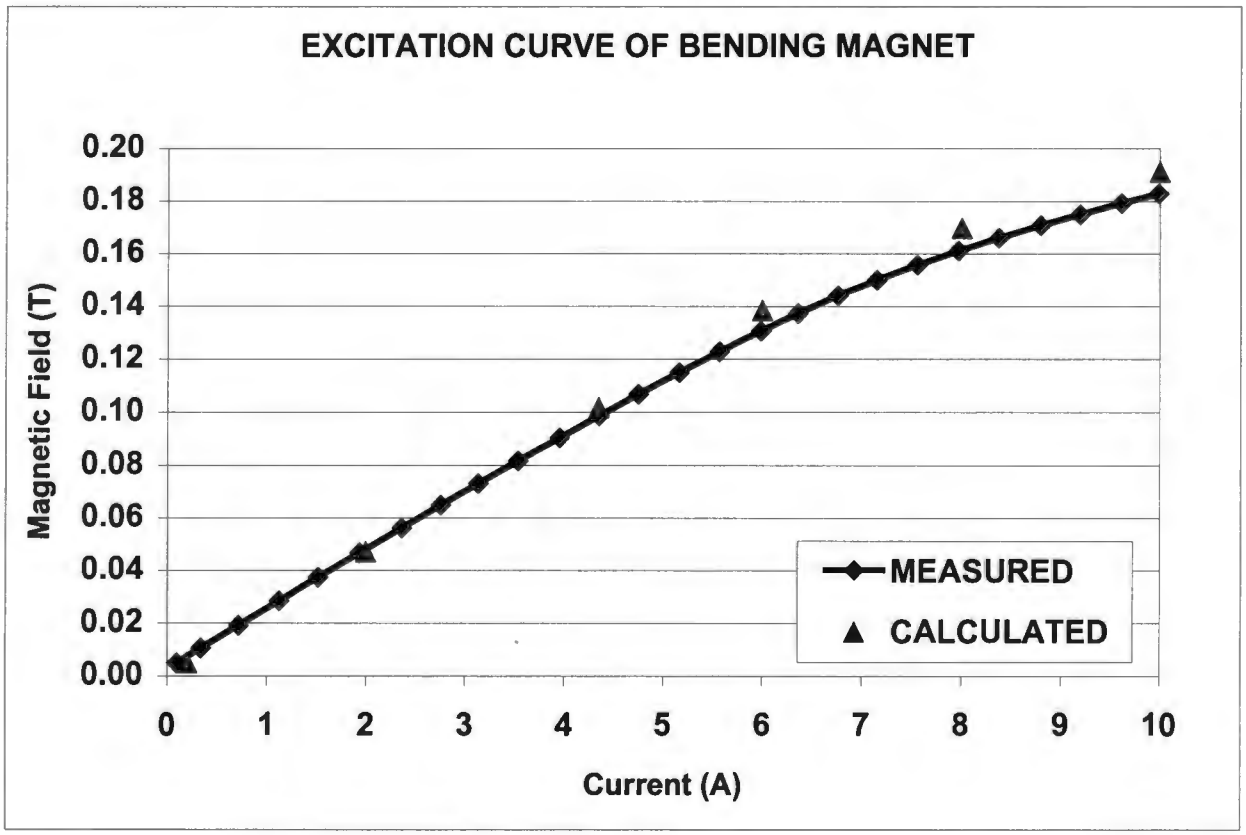

Fig.6.5: The measured excitation curve of the bending magnet compared with a few calculated values.

- **The magnetic field along longitudinal axis through the magnet**

Figure 6.6 shows the calculated and measured axial magnetic field component along a longitudinal path in the magnetic median plane. This shows the shape of the edge fields and also the homogenous nature of the magnetic field along a path through the magnet.

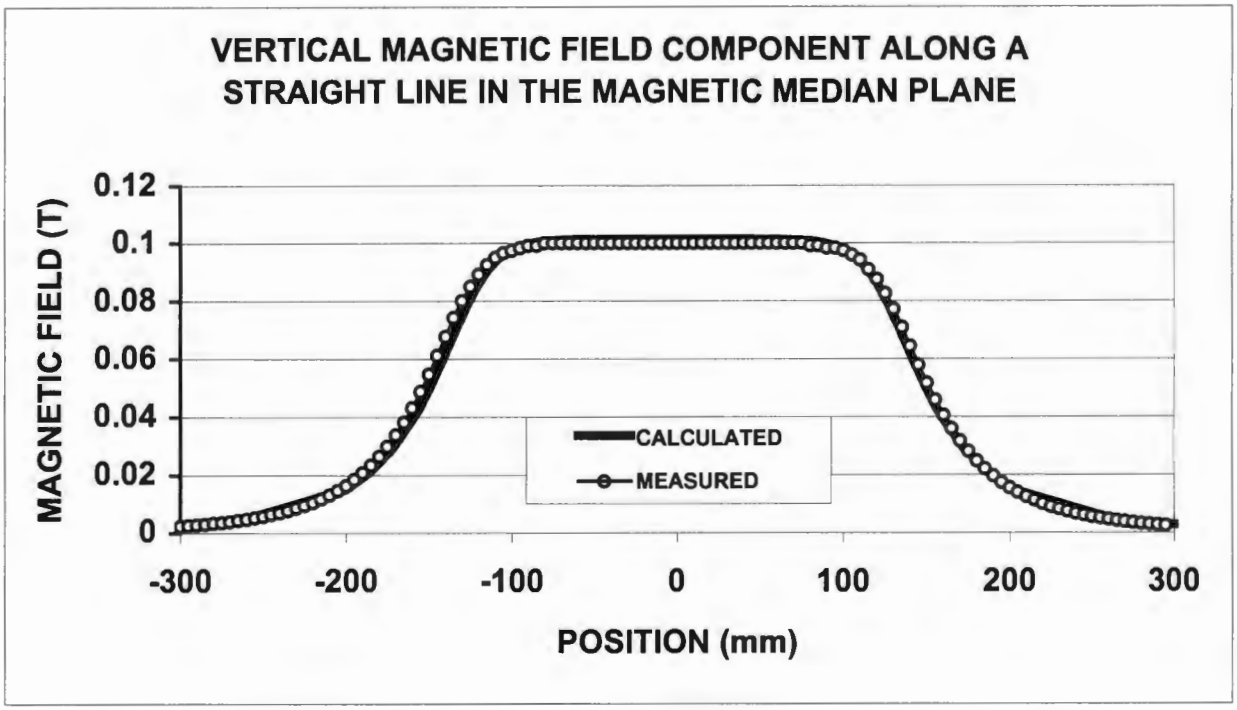

Fig.6.6: The calculated and measured main field component along a straight line through the magnet in the magnetic median plane.

- **Homogeneity of the field**

Iterative calculated changes to the geometry of the side shims resulted in an optimum geometry, which provides the best transversal magnetic field homogeneity. Figure 6.7 shows a side view section of the pole plates and shims through the centre of the magnet (the beam direction is perpendicular to the paper). The magnetic field distribution is also shown in relation to the displayed geometry. The shims cover the full length of each side of the pole plate with an optimised width of 15 mm and height of 2.5 mm. The deviation of the magnetic field over 75% pole width was calculated to be less than 2% of the maximum field value as shown in figure 6.8. A field deviation of 2% is acceptable for the present purpose of the magnet. The deviation over 50% of the pole width is less than 0.2%.

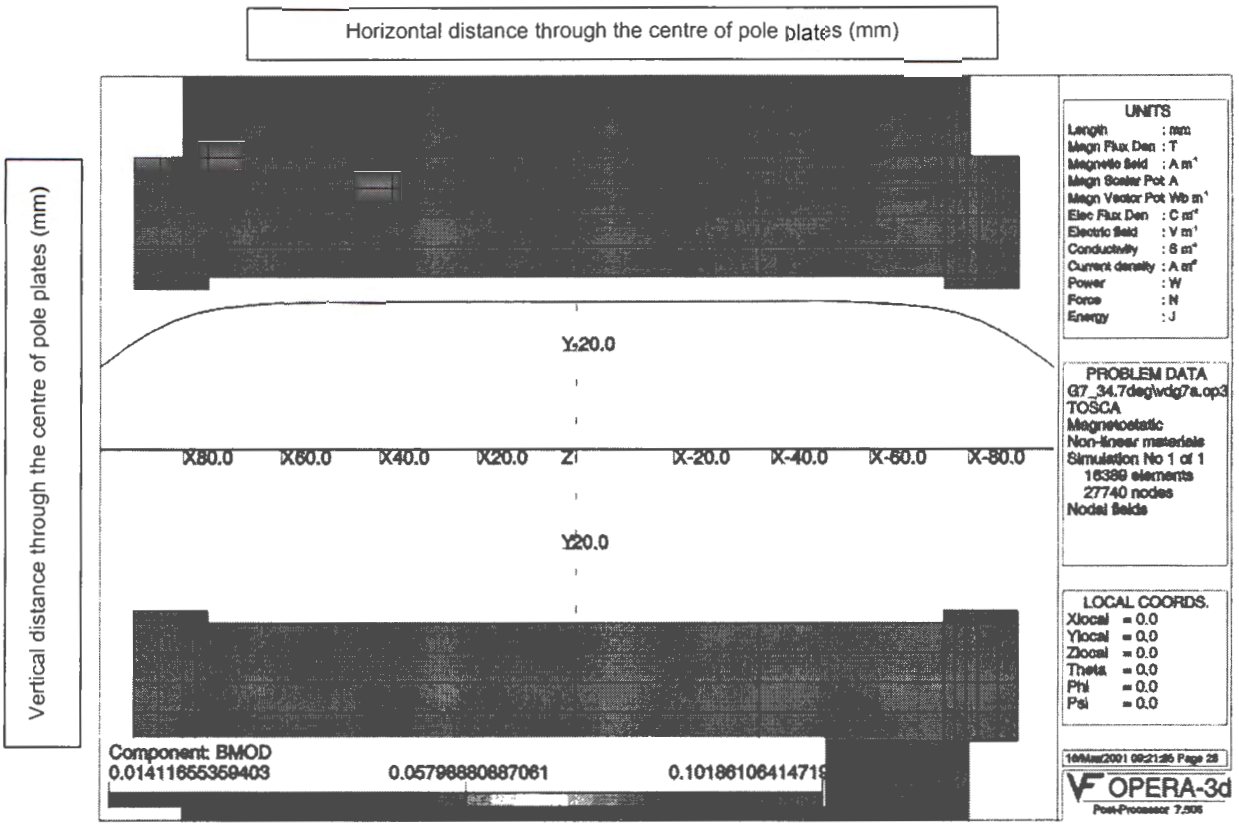

Figure 6.7: A side view section through the centre of the pole plates and side shims of the calculated magnet, with the calculated transversal field shape shown in relation to the geometry, and the maximum field strength is about 0.1T.

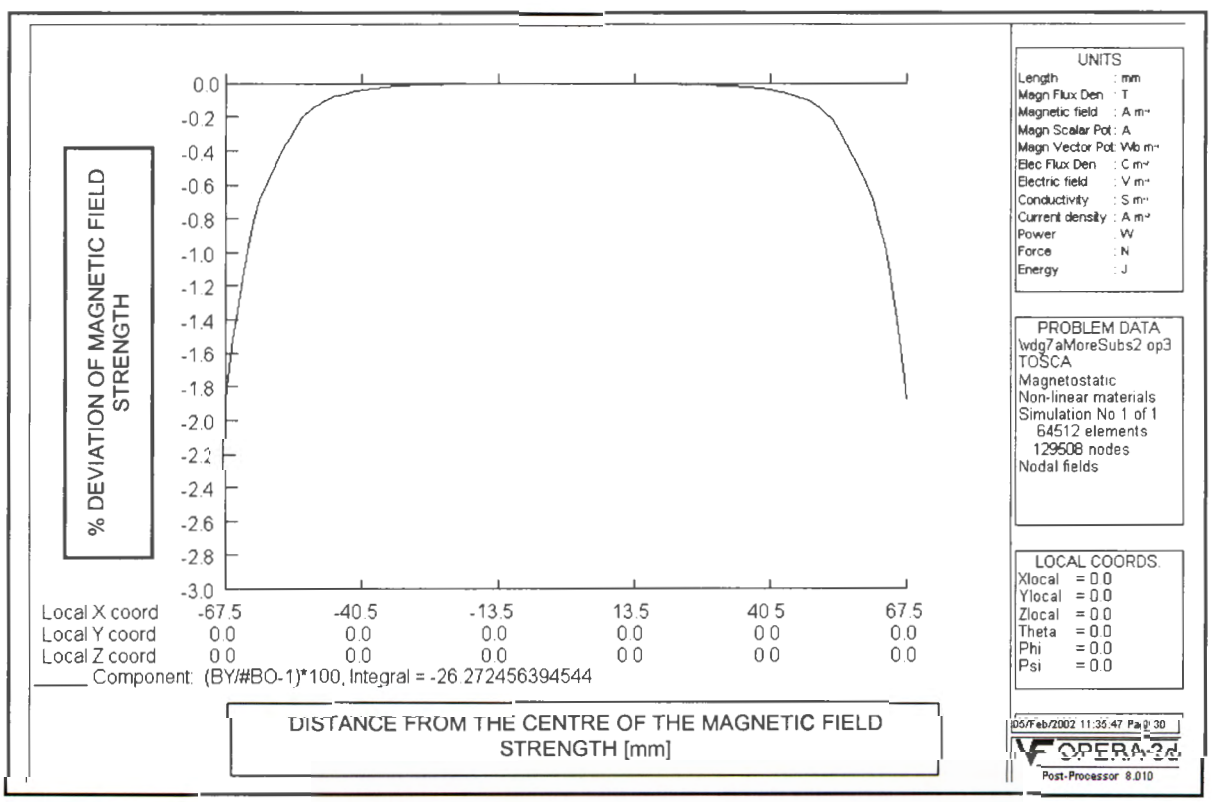

Figure 6.8: Variation in the magnetic field strength over 75% of the width of the pole plate, in the median plane and on the longitudinal mirror plane. The maximum deviation is less than 2% of the maximum field value.

♦ Effective Length

According to Parzen **[PAR76]** the effective length (L_{eff}) of a magnet (i.e. region in the magnet median plane through which the magnetic field is almost constant) with pole length, L, and pole gap, g, is approximately given by the following expression:

$$L_{eff} = \Delta L + L \tag{6.23}$$

where ΔL/2, the contribution of one end to the effective length for an H-magnet, may lie between,

$$\frac{\Delta L}{2} = 1.1g = 77mm \text{ and}$$

$$\frac{\Delta L}{2} = 0.63g = 44.1mm .$$

This yields the following values of L_{eff} for the bending magnet:

$$\Rightarrow \qquad L_{eff} = \begin{cases} 410mm \\ 344mm \end{cases}$$

The calculated and measured effective lengths of the magnet are given in table 6.1. The measured value for effective length of the magnet and the value calculated with TOSCA are approximately 320 mm. The empirical formulas of Parzen give values in excess of 340 mm for a magnet pole gap of 70 mm and a pole length of 256 mm.

TABLE 6.1: CALCULATED AND MEASURED EFFECTIVE LENGTHS OF THE MAGNET.

EFFECTIVE LENGTH OF THE BENDING MAGNET			
METHOD	NUMERICAL FIELD ANALYSIS WITH TOSCA	MEASURED	EMPIRICAL FORMULA OF PARZEN
EFFECTIVE LENGTH (mm)	320	324	344 – 410

The magnet characteristics are summarised in table 6.2.

TABLE 6.2: CHARACTERISTICS OF THE ANALYZING MAGNET.

Bending angle	90^0
Bending radius	220 mm
Edge angle	34.7^0
Magnetic rigidity	0.0204 Tm
Effective length of the magnet (measured)	324 mm
Pole width	110 mm
Pole gap	70 mm
Magnetic field in the pole gap at 6 A	0.1 T
Yoke thickness	20 mm
Width of side shims	15 mm
Height of side shims	2.5 mm

Total number of windings (4 coils x 330 turns)	1320
Nominal coil wire diameter	2 mm
Maximum coil current density	2 A/mm^2
Electrical coil resistance	2.23 Ω
Maximum coil current (without additional cooling)	6 A
Voltage drop over coils	13.38 V
Power consumption of coils	80.28 W

Energy resolving power for 10 mm object slit	1.832%
Mass resolving power for 10 mm object slit	1.832%
Momentum resolving power for 10 mm object slit	0.916%
Charged states selection for 10 mm object slit	1 in 5

6.5 CONCLUSION

TOSCA has shown to be very useful for designing and optimisation of the 90^0 bending magnet. The results obtained from the numerical field analysis method, not only confirms what can be obtained with the analytical expressions derived for the design of the bending magnet geometry, but is essential for effective optimisation of the magnetic fields in a cost effective manner.

The saturation effects of the magnetic field is found to be negligible even at higher than required excitations of the coil and the magnetic field homogeneity in the beam region between the pole plates is within 2% from the maximum field value.

The measured effective length of the magnet corresponds very well to the value calculated with the numerical field analysis method. The deviation of the results obtained with the empirical formula can mainly be ascribed to the relatively large pole gap of the magnet.

The higher order multipole-effects of the present design, were not studied, but will have to be done for further optimisation of the magnet geometry.

CHAPTER 7

IMPROVEMENT OF THE ENERGY RESOLUTION OF THE VAN DE GRAAFF BEAMLINES

7.1 INTRODUCTION

The Van de Graaff accelerator and its beamlines have been briefly discussed in chapter two. With the current beamline design, which dates back to 1962, the energy resolution is about 1%. Initially there was no need for better energy resolution, but in recent years, with the acquisition of the multi-probe facility and the stronger emphasis on solid state physics experiments, the demand for beams with high energy-resolution increased.

To obtain high energy resolution in a beamline at least one double-focusing bending magnet, with a large radius, as well as object and image slits, on which the beam should be focused, are required. A 90^0 bending magnet with variable entrance and exit edge angles, which can be set for double focusing, is available in the existing beamline. There is, however, no object slit and the slit after the bending magnet is not at the image position. In the existing beamline it is also not possible to focus the beam at the position where the object slit should be.

The basic theory of an energy analyzing system, comprising of a bending magnet and object and image slits, as well as the redesign of the Van de Graaff accelerator beamlines to increase the energy resolution will be discussed in this chapter. The computer program TRANSPORT will again be used for beamline design. Since the horizontal and vertical beam emittances at the exit of the Van de Graaff accelerator are not known, the method of simultaneously fitting several sets of measured profile data with the program TRANSPORT will be used to determine these all important values.

7.2 THE BEAM EMITTANCE

7.2.1 THE METHOD USED TO DETERMINE THE BEAM EMITTANCE

In order to design a new beamline the beam characteristics at the entrance to the beamline, e.g. the size and orientation of the areas occupied by the beam in the horizontal, vertical and longitudinal phase space planes, as well as the different required waist conditions along the beamline have to be specified. The fields and field gradients of the beamline components are then varied in order to obtain the desired beam characteristics along the beamline. The computer program TRANSPORT is very useful for this purpose because it has powerful fitting capabilities, which are usually applied when a new beamline is designed.

Conversely, for an existing beamline with some profile monitors TRANSPORT may also be used to find the initial conditions by making use of the measured profile data. In practice this is done by using the measured beam half-widths as constraints and by freeing the appropriate variables of the initial beam in the program. If there are three or more measured widths per direction, the correlation coefficients may also be freed. The actual field and field gradient values of beamline components have also to be inserted at the appropriate places. Another method is to measure the beam profiles for several different settings of the same beamline components and for the same initial beam conditions and then perform a simultaneous multi-envelope fit with TRANSPORT to determine the beam characteristics in phase space at the entrance to the beamline. Simultaneously fitting of calculated to several sets of measured beam profile data with the program TRANSPORT, is an excellent way of accurately determining the emittance of a given beam.

7.2.2 DETERMINATION OF THE EMITTANCE OF THE BEAM FROM THE VAN DE GRAAFF ACCELERATOR

To determine the emittance of the beam from the Van de Graaff accelerator a combination of the two methods described above has been used. The beam widths were measured for different entrance and exit edge angles of the 90^0 bending magnet with a slit directly after the bending magnet and a rotating scanner at a distance of about 1.1 meter downstream from the slit. The beam profiles from the scanner were displayed on a digital oscilloscope and were transferred from the oscilloscope to a personal computer. A computer program, SIGMAPLOT, was used to obtain a distribution function of the measured beam profiles and to remove the unwanted noise. The best Gaussian fit is given by:

$$y = a + b\exp\left[-0.5\left(\frac{x-c}{d}\right)^2\right] \qquad (7.1)$$

where,

x and y are the deviation and probability density factors of the beam distribution,

a a parameter representing the extent in which the beam size is displaced on the (x and y) axis,

b a factor that ensures that $\int_{-\infty}^{+\infty} y dx = 1$, i.e. a normalisation factor,

c the mean of the beam distribution, i.e. the beam center, and

d the root mean square beam size and characterises the width of the beam distribution, i.e. the standard deviation.

The width of the beam profile is given by the parameter d, the equivalent of sigma used in chapter 3. Figure 7.1 shows a beam profile measured with the scanner for entrance and exit edge angles of 5^0. Also indicated in figure 7.1 is the associated Gaussian distribution calculated with the program SIGMAPLOT. From the figure it is clear that a Gaussian distribution is a good approximation of the measured beam profile. The beam widths are obtained from a Gaussian approximation to the measured data.

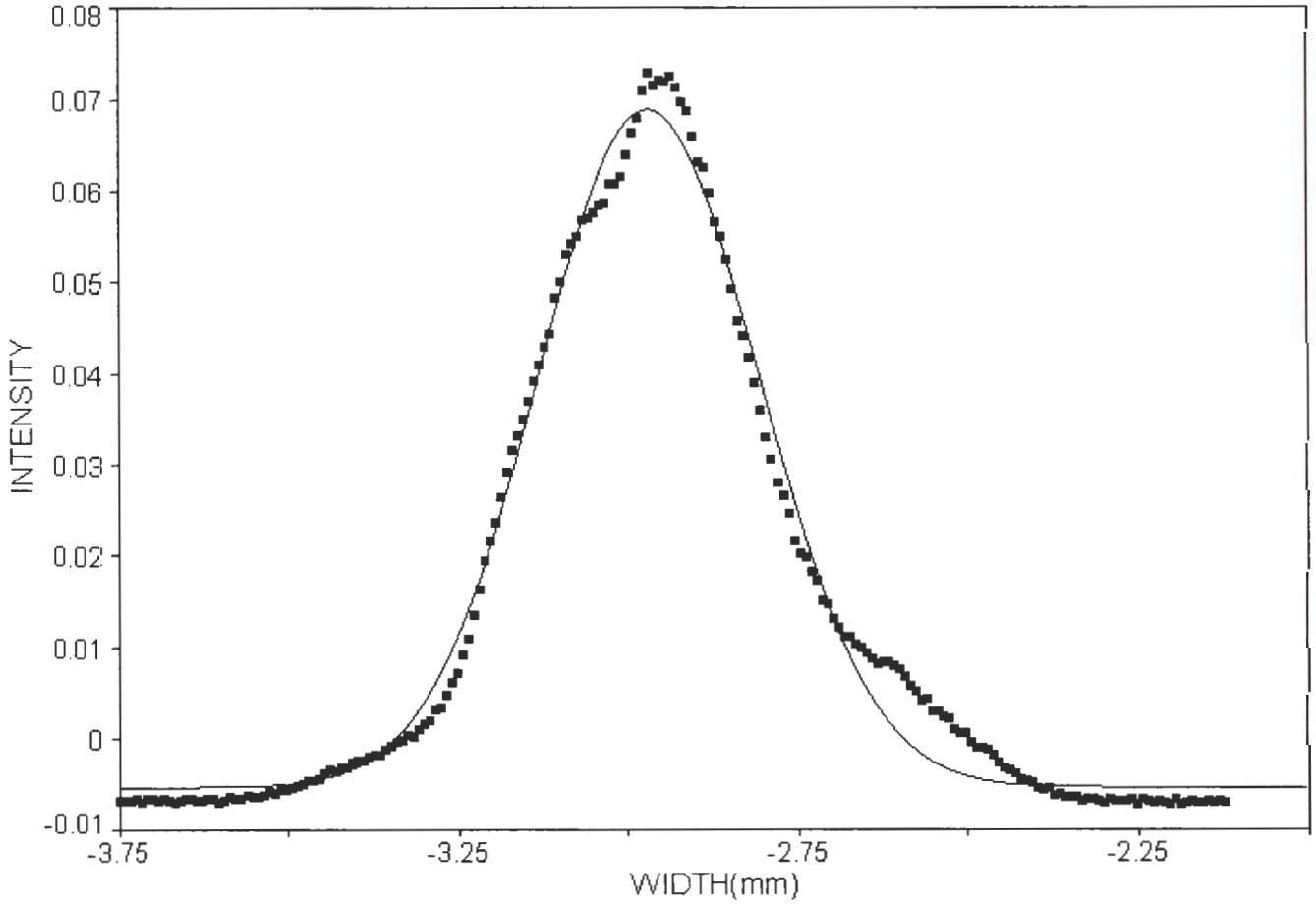

[▮▮ measured and — Gaussian fit]

Fig.7.1: Typical measured vertical beam profile and its Gaussian fit distribution.

Table 7.1 provides the parameters of equation (7.1) for both the horizontal and vertical Gaussian distribution functions of the beam.

TABLE 7.1: RESULTS OF BEAM PROFILE MEASUREMENTS FOR BOTH THE VERTICAL AND THE HORIZONTAL DIRECTIONS.

VERTICAL

a (mm)	**b** (mm)	**c** (mm)	**d** (mm)	**Angle** (degrees)
-0.003937	0.05561	-2.9675	0.4878	5
-0.002491	0.05185	-3.1204	0.3206	15
-0.002274	0.03097	-3.1780	0.2890	20
-0.002490	0.05480	-3.2555	0.2793	25
-0.004977	0.07644	-3.2494	0.3347	30
-0.005115	0.07113	-3.3192	0.3371	35

HORIZONTAL

a (mm)	**b** (mm)	**c** (mm)	**d** (mm)	**Angle** (degrees)
-0.005001	0.09786	3.19504	0.28929	5
-0.002628	0.10435	3.17892	0.17859	15
-0.002388	0.05707	3.23482	0.16874	20
-0.002432	0.10302	3.17263	0.16080	25
-0.004615	0.13078	3.11433	0.20681	30
-0.004776	0.10430	3.08141	0.22269	35

The beam width, parameter d in table 7.1, for the vertical and horizontal distributions, is required for running the program TRANSPORT in order to obtain the beam characteristics. The beam sigma matrix, shown in table 7.2, describes the beam characteristics at the position where the object slit should be, in front of the bending magnet.

TABLE 7.2: THE ELEMENTS OF THE BEAM SIGMA MATRIX FOR THE EMITTANCE MEASUREMENTS AS CALCULATED WITH TRANSPORT.

		x	θ	y	ϕ	ℓ
x	$\sqrt{\sigma_{11}}$ =2.595 mm					
θ	$\sqrt{\sigma_{22}}$ =1.439 mm	r_{21}=-0.861				
y	$\sqrt{\sigma_{33}}$ =4.859 mm	r_{31}=0.000	r_{32}=0.000			
ϕ	$\sqrt{\sigma_{44}}$ =2.340 mm	r_{41}=0.000	r_{42}=0.000	r_{43}=-0.883		
ℓ	$\sqrt{\sigma_{55}}$ =0.627 mm	r_{51}=0.000	r_{52}=0.000	r_{53}=0.000	r_{54}=0.000	
δ	$\sqrt{\sigma_{66}}$ =0.000 %	r_{61}=0.000	r_{62}=0.000	r_{63}=0.000	r_{64}=0.000	r_{65}=0.000

The simultaneous multi-envelope fit for the calculated sigma matrix is shown in figure 7.2. For this calculation, the exit edge angle of the 90^0 bending magnet was varied. The exit edge values used were 5^0,15^0 ,20^0 ,25^0 ,30^0 and 35^0, and the entrance edge angle was fixed at 27^0 for all the measurements. The "T" and inverted "T" characters in figure 7.2 indicate the constraints that were used to fit the horizontal and vertical beam envelopes, respectively. The TRANSPORT input file used for the simultaneous multi envelope fit for the emittance determination of the Van de Graaff accelerator is given in appendix D.

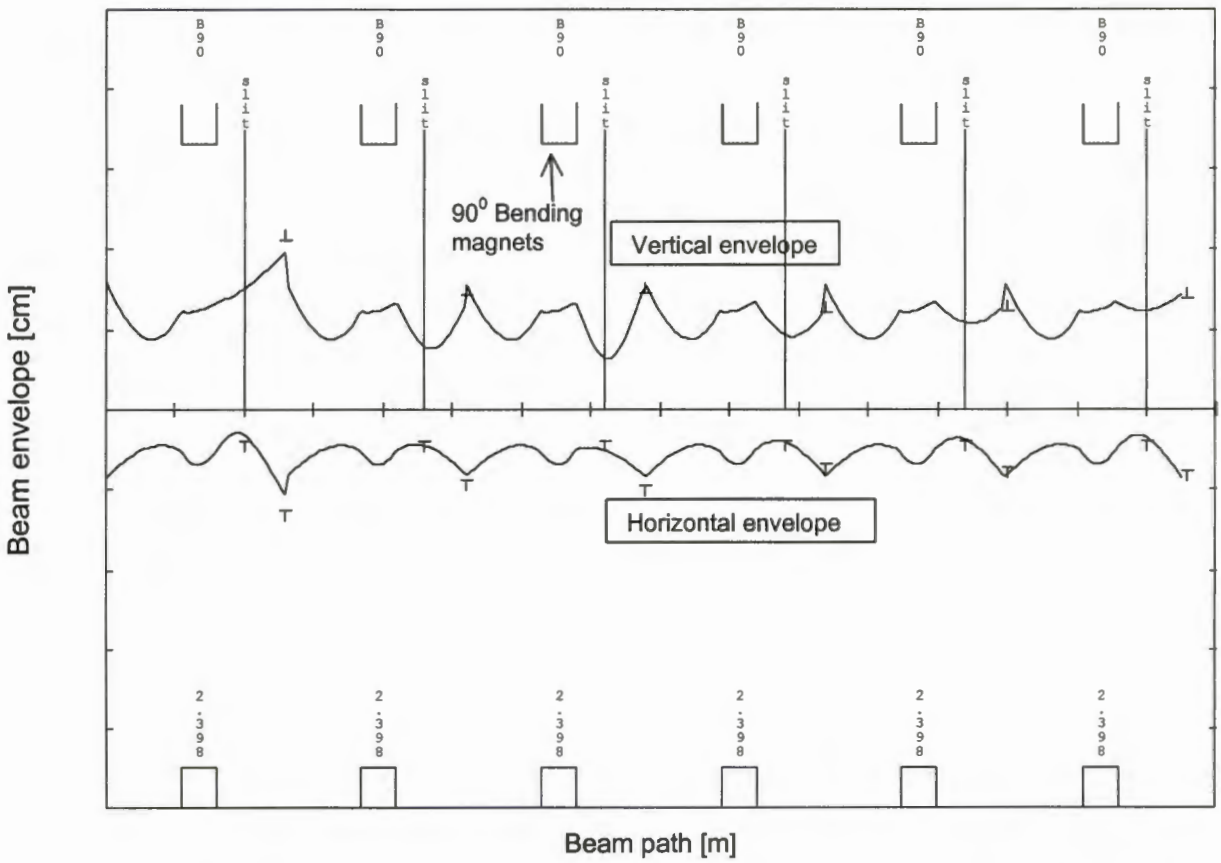

Fig.7.2: Simultaneous beam envelope fit for determining the beam emittance of the Van de Graaff accelerator.

From the results of table 7.2, the horizontal and vertical beam emittances, ε_x and ε_y, were calculated using the following expressions (3.18):

$$\varepsilon_x = \pi\sqrt{\sigma_{11}\sigma_{22}\left(1 - r_{12}^{\ 2}\right)}$$

$$= \pi\sqrt{(2.595)^2(1.439)^2\left(1 - (-0.861)^2\right)}$$

$$= 1.899\pi \text{ mm mrad}$$

and,

$$\varepsilon_y = \sqrt{\sigma_{33}\sigma_{44}\left(1 - r_{34}^{\ 2}\right)}$$

$$= \sqrt{(4.859)^2(3.340)^2\left(1 - (-0.883)^2\right)}$$

$$= 7.617\pi \text{ mm mrad}$$

The emittance of the beam in the y-direction is large compared to that of the x-direction due to the dispersion introduced into the beam by the 90^0 bending magnet. These emittance values and the sigma matrix, given in table 7.2, will further be used in the calculations for optimisation of the remaining beamlines.

7.3 BEAMLINE DESIGN

The new layout of beamlines at the Van de Graaff accelerator is shown in figure 7.3. The following proposed modifications to the beamlines, to increase the energy resolution and to focus the beamline to the desired beam spot size, are indicated in the figure:

- Installation of two additional quadrupole magnets, immediately after the Van de Graaff accelerator, to focus the beam at the object position of the bending magnet.
- Installation of a slit at the object position of the 90^0 bending magnet.
- Adjustment of both the entrance and exit edge angles of the bending magnet to 27^0 for double focussing of the beam.
- Installation of the existing slit at the image position of the bending magnet for energy selection.
- Installation of another quadrupole magnet in front of the switcher magnet to match the beam from the modified beamline to the remaining lines.

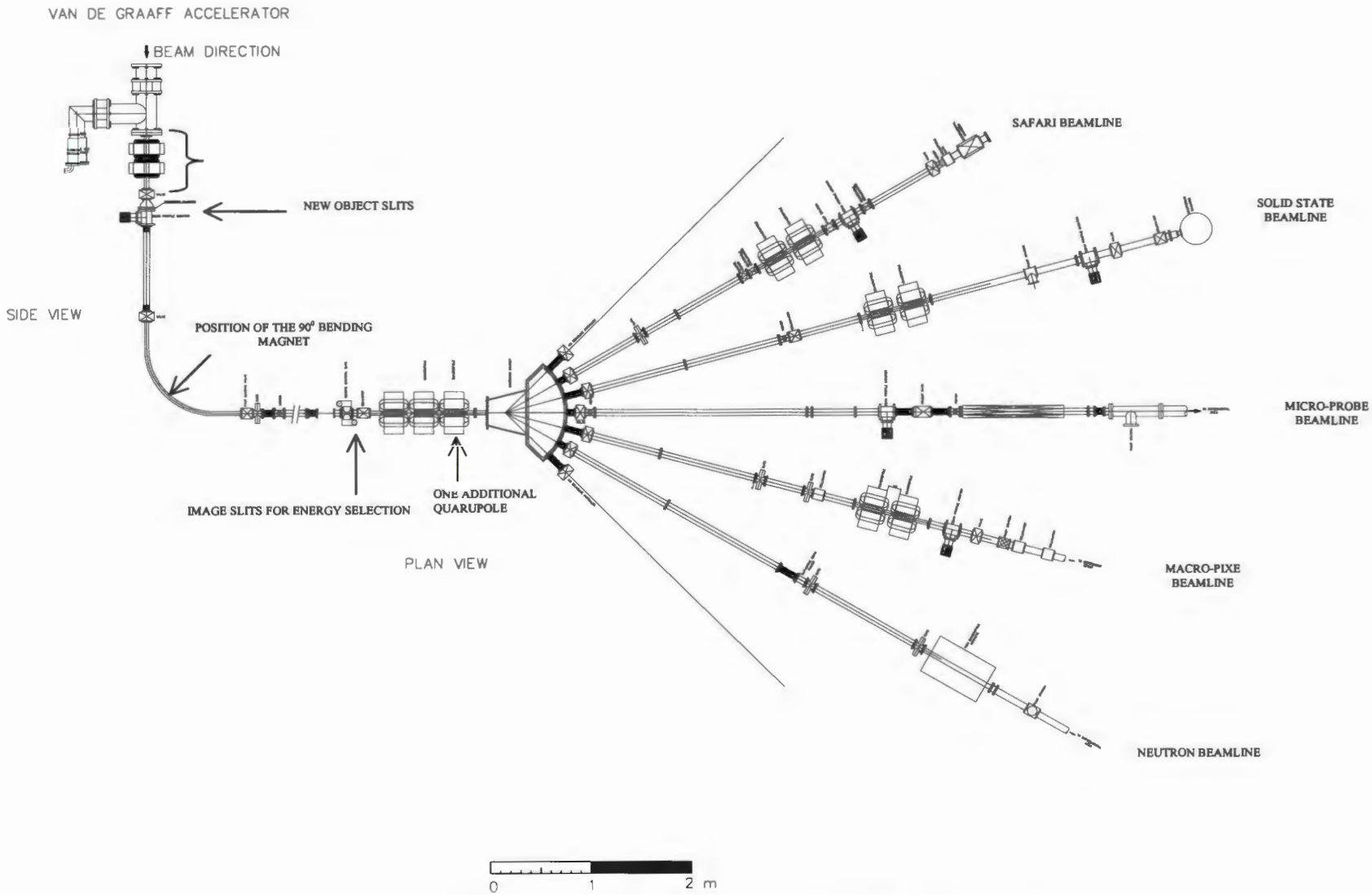

Fig.7.3: Layout of the redesigned beamlines at the Van de Graaff accelerator.

The TRANSPORT input file used for the redesigned beamline up to the target position in the Safari beamline is given in appendix D. The files for the remaining beamlines are similar, but with different quadrupole settings. For the other beam profiles, the beam line is shown (in appendix D) appearing five times with the same beam and correlation cards, but with different quadrupole gradients and measured profile data. The five different sets of field values for the quadrupoles Q1 to Q7 are listed.

The fields and the gradients of different magnetic beamline elements were varied in order to obtain transmission through the beamline and beam waists at the desired positions. This was done to obtain a good fit to the measured beam widths and to verify that we know the parameters of the beamline. The beam envelopes fits for the redesigned beamlines are shown below in figures 7.4 to 7.8. The beam envelopes are satisfactory and show consistency.

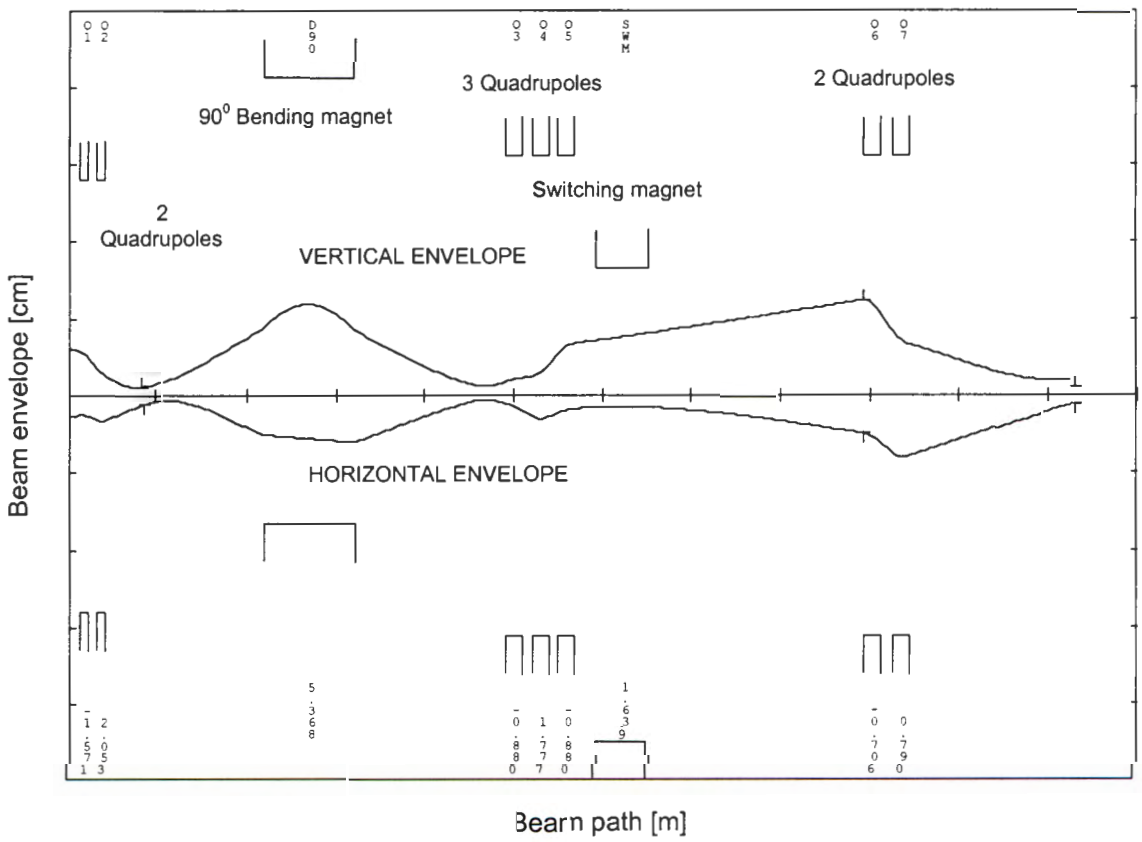

Fig.7.4: The calculated beam envelope for the redesigned Safari beamline.

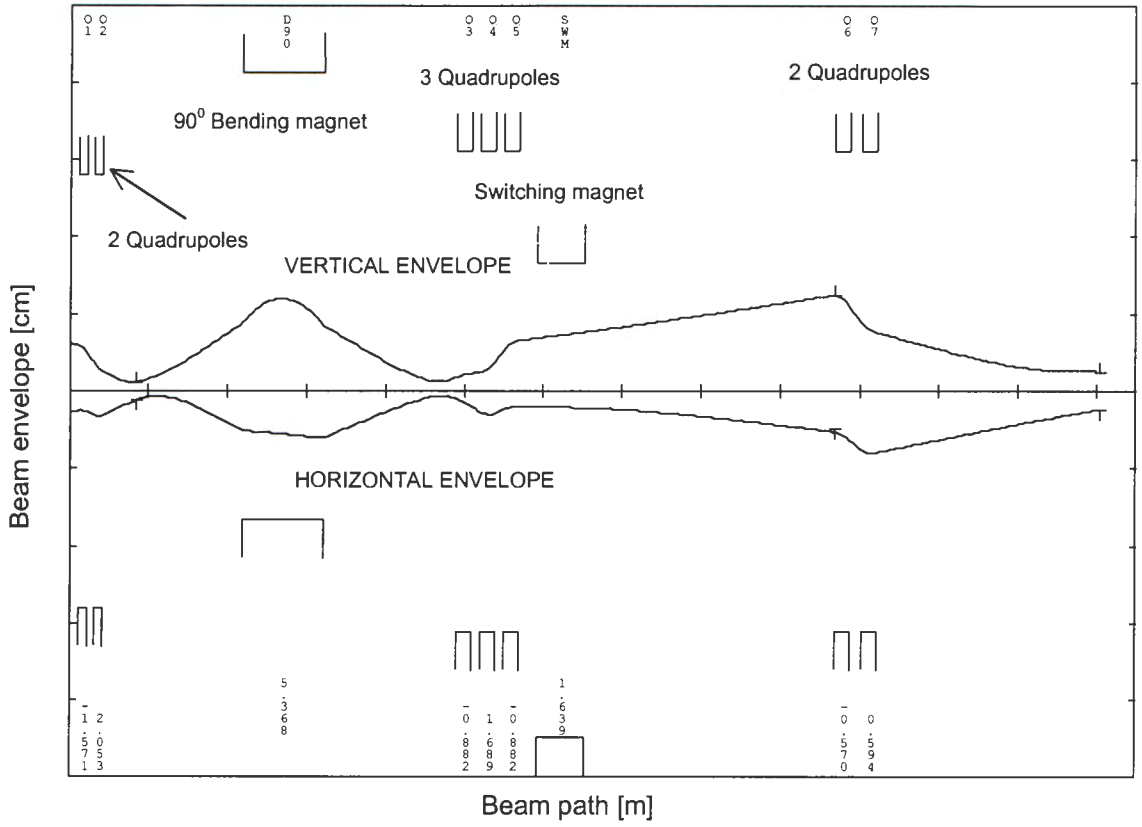

Fig.7.5: The calculated beam envelope for the redesigned Solid State beamline.

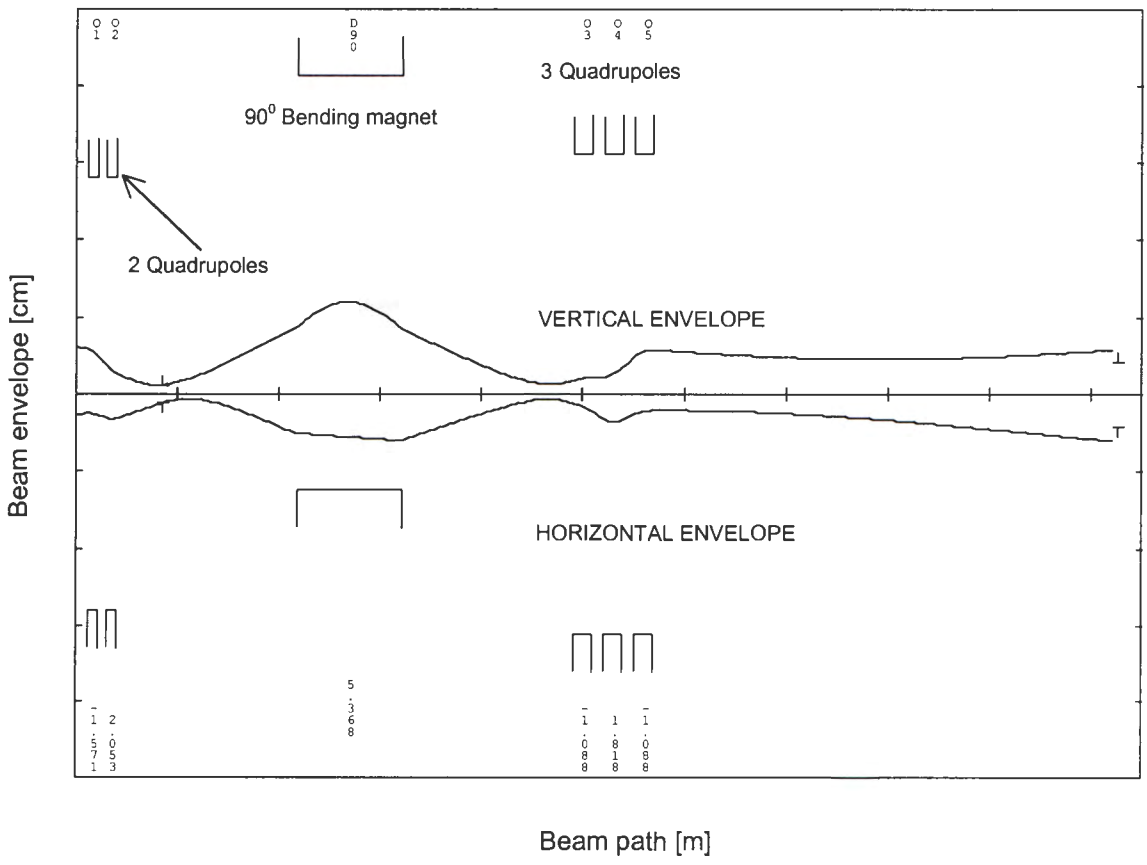

Fig.7.6: The calculated beam envelope for the redesigned Micro-probe beamline.

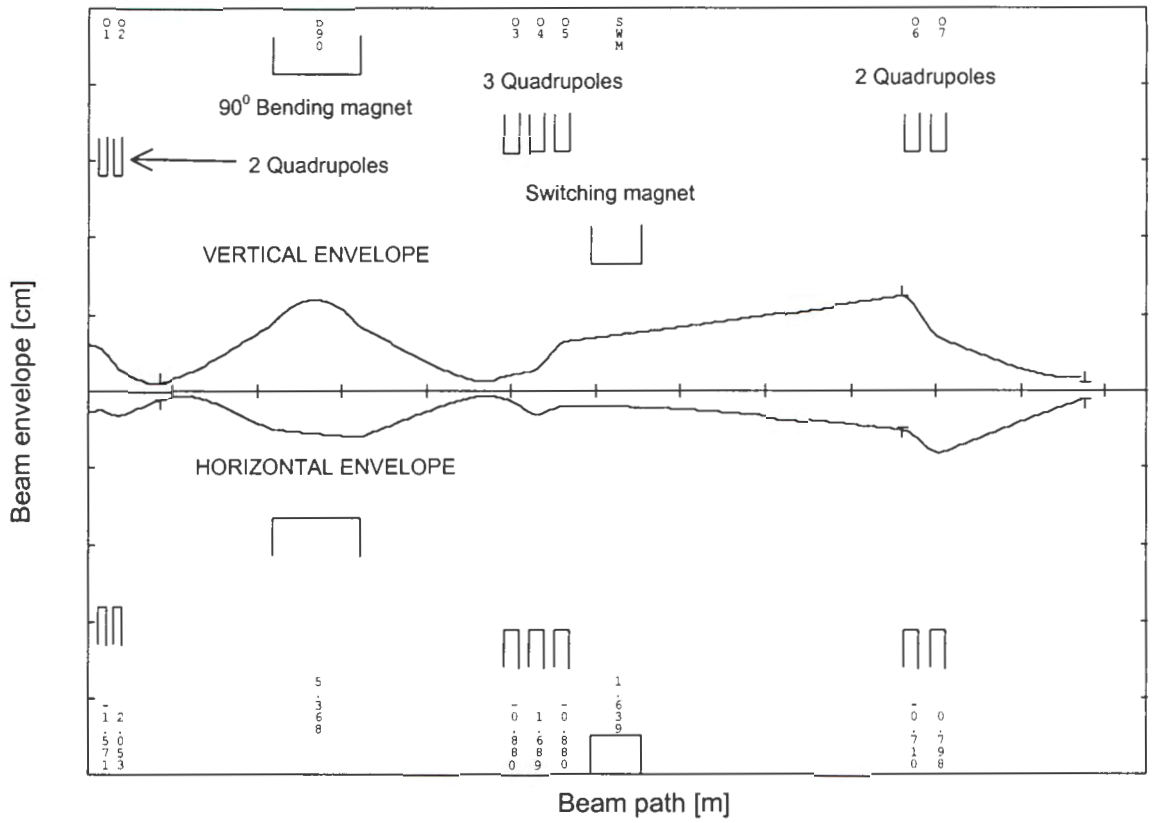

Fig.7.7: The calculated beam envelope for the redesigned Macro-PIXE beamline.

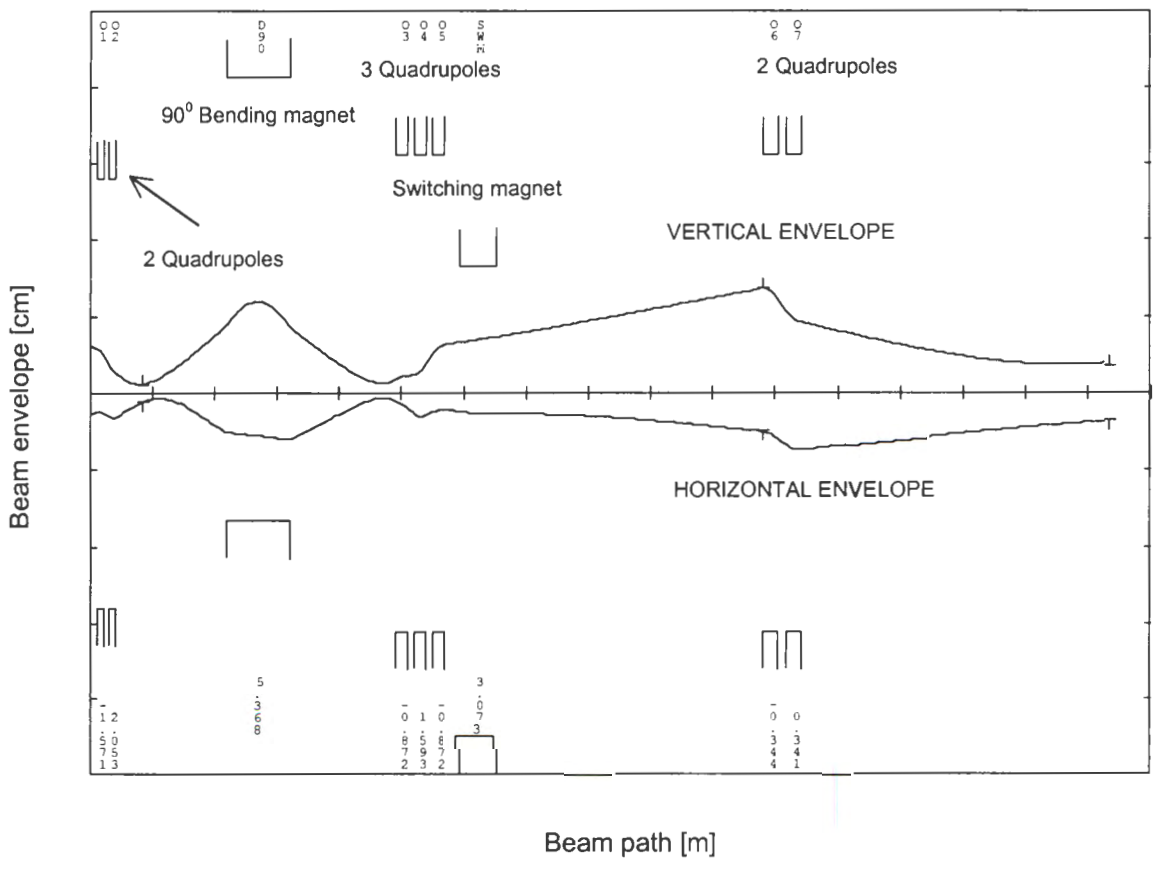

Fig.7.8: The calculated beam envelope for the redesigned Neutron beamline.

7.4 THE ENERGY RESOLUTION OF THE NEW BEAMLINE DESIGN

For a bending magnet with an object and image slit, the energy resolution at low energies ($E<<E_0$) is given by equations (6.17) and (6.18):

$$\frac{\Delta E}{E} = 2\frac{\Delta p}{p} = \frac{4R_{11}w}{R_{16}} \tag{7.2}$$

with w being the width of the object and image slits.

R_{11} and R_{16} can be calculated from equations (6.20) and (6.22). For a bending magnet with a radius of 0.66 m, entrance and exit edge angles of 27 degrees, the calculated R_{11} element is –0.9712 and R_{16} element 2.652 cm/%. The TRANSPORT elements R_{11} and R_{16} are –0.97128 and 2.6528 cm/%, respectively, and are comparable to the calculated values. Thus the momentum resolution for a 1mm object and image slit is:

$$\frac{\Delta E}{E} = 2\frac{\Delta p}{p} = 4 \times \frac{0.9712}{2.652} \times 0.1$$

$$= 0.146\%$$

In the current momentum analysing system the analysing slit is not at the image point and there is no object slit. Thus, the momentum resolution of the system depends on the width and divergence of the beam at the object point. A direct comparison between the proposed system and the current system is thus not straightforward. For a beam with a beam width of 5 mm and divergence of 8 mm at the object point, the momentum resolution with an image slit of 1 mm is about 1% as determined with the computer program TURTLE **[PBO2.0]**. For this specific case, the proposed analysing system is about a factor of 7 better than the existing one.

The proposed system thus gives a big improvement in the momentum resolution. The momentum resolution of the system is also independent of the beam parameters; it is only a function of the gap size of the object and image slits. With the current system the beam parameters can influence the momentum resolution of the system dramatically.

7.5 CONCLUSIONS

Calculations on the Van de Graaff beamlines, using the program TRANSPORT and emittance data obtained by fitting measured to calculated beam profiles, have shown that with two additional quadrupole magnets and a slit the energy resolution can be improved from 1% to 0.15%. These modifications will not only result in better energy resolution but also in improved transmission efficiency in all the beamlines. Beams of adequate intensity and quality will be available. The information about the beam and beamlines obtained in the course of this work will serve as a basis for future analysis of the beamlines and for matching the beam from the Van de Graaff accelerator to the beam requirements at the targets of the different user groups.

CHAPTER 8

DISCUSSION AND CONCLUSIONS

A suitable position for coupling a third external ion source for high-intensity proton beams to the injection beamlines of SPC2 has been found. A double focusing 90^0 bending magnet, for separation of the proton beam from unwanted molecular hydrogen ions has to be inserted between the source and the existing beamlines. Because of space limitations the bending magnet will also be used to focus the beam in both the horizontal and vertical directions. By calculation, using the program TRANSPORT, the best position for the ion source with respect to the magnet has been determined. Satisfactory beam envelopes could be obtained with the existing beamline elements up to the centre of SPC2. This shows that except for the bending magnet no further beamline elements are required to inject a beam from the new source into SPC2. The field strengths of solenoid L8H and the beamline elements in the AX-beamline required for operation with the duoplasmatron ion source have been calculated.

Approximate analytical expressions were used to design and optimize the dimensions of the 90^0 bending magnet. An H-type magnet with a bending radius of 220 mm and a pole gap of 70 mm were decided upon. The calculated double focusing distance of 525 mm is acceptable for beam focusing. More accurate field calculations performed with the commercially available computer program TOSCA, which uses finite element analysis, verified the results obtained with analytical expressions and was used to optimise the entrance and exit angles of for the magnet poles to a value of 34.7^0. Saturation effects are negligible even at higher than required excitations of the coil and the field homogeneity in the beam region between the pole plates is better than 2% of the maximum field value.

The Van de Graaff beamlines were redesigned to improve their energy resolution and the quality of the beams delivered to the different users. Calculations, using the computer program TRANSPORT and emittance data obtained by fitting measured to calculated beam profiles, have shown that with two additional quadrupole magnets and a slit, the energy resolution can be improved from 1% to 0.15%. This modification will not only result in better energy resolution but also in improved

transmission efficiency in all the beamlines. Beams of adequate intensity and quality will become available when the proposed modifications are implemented. The information about the beam and beamlines obtained in the course of this work will be used in future for further analysis of the beamlines and for matching the beam from the Van de Graaff accelerator to the beam requirements at the targets of the different user groups.

In the course of this work experience was gained on several aspects of accelerator science such as the design of beamlines and beamline elements and the calculation of magnetic fields, respectively with the available computer programs, TRANSPORT and TOSCA.

APPENDIX A

MAIN CHARACTERISTICS OF THE CYCLOTRONS AT iThemba LABS

SSC:

Parameters	Values
K-value	200 MeV
Injection radius	1.01 m
Extraction radius	4.43 m
Largest diameter	13.2 m
Magnetic flux density	1.26 T
Magnet sectors	4 x 34^0 sectors
Resonators	2 x 49^0 deltas, $\lambda/2$
Dee voltage	250 kV (maximum)
RF power consumption	80 kW/resonator
Frequency range	6 – 27.5 MHz
Harmonic numbers	4 & 12
Frequency variation	Short-circuit plates & variable capacitors
Power amplifier	130 kW

SPC1:

Parameters	Values
K-value	8 MeV
Extraction radius	0.476 m
Magnetic flux density	0.86 T (max.)
Number of sectors	4
Resonators	2 x 90^0 dees, $\lambda/4$
Frequency range	8.6 – 27.5 MHz
Harmonic numbers	2 & 6
Internal ion source	PIG source

SPC2:

Parameters	Values
K-value	10 MeV
Extraction radius	0.476 m
Magnetic flux density	0.86 T (max.)
Number of sectors	4
Resonators	2 x 90^0 dees, $\lambda/4$
Frequency range	8.6 – 27.5 MHz
Harmonic numbers	2 & 6
External ion sources	ECR & polarised hydrogen ion sources

APPENDIX B

THE TRANSPORT INPUT FILE USED FOR THE DESIGN OF THE BEAMLINE BETWEEN THE DUOPLASMATRON ION SOURCE AND SPC2 (20 KeV) IS HENCEFORTH LISTED:

/Beamline Between Duoplasmatron Ion Source & SPC2, 20 keV protons/

```
0 (Indicator card: means the data that follows describes a new problem)
13. 48.0 /ANG/ ;                    (Bending magnet input specification)
15. 1.0 /mm/ 0.1                    (Input-output units)
16. 22. 300. /NITR/ ;               (number of steps for random search)
-16. 31. 0. /RANO/;                 (switch to random search algorithm)
1. 3 67 3 67 .9 .0 .005462 ;        (initial beam parameters)
16. 7.0 .7 ;                        (first fringe field correction coefficient of bending
                                     magnet)
16. 8.0 4.4 ;                       (second fringe field correction coefficients)
3. .11 /L1/ ;                       (drift space)
16. 5.0 47 ;                        (vertical half-aperture of bending magnet, gap.)
2. 28 /EA1/  ;                      (angle of pole-face rotation, degrees)
4. .220 90. 0.  /Bend/ ;            (90° bending magnet)
2. 23 /EA2/  ;
3. 1.544 /L2/ ;
16. 5.0 40 ;
19.00 .075  2.2 /L8H/ ;             (solenoid)
3. .385 /L3/ ;
10. 1.0 1.0 6 .0001 /HWA2/ ;        (fitting constraint for parallel to point focus, horizontal
-10. 3.0 3.0 6 .0001 /VWA2/ ;       ,HWA2, & vertical ,VWA2,.planes for L8H)
13. 1.0 ;                           (prints the current beam matrix)
3. .0345 /L4/ ;
5. .176 .279 52.5 /Q1AX/ ;
3. .024 /L5/ ;
5. .176 -.479 52.5 /Q2AX/ ;
3. .024 /L6/ ;
5. .176 .279 52.5 /Q3AX/ ;
3. .389 /L7/ ;
5. .176 .279 52.5 /Q4AX/ ;
3. .024 /L8/ ;
5. .176 -.479 52.5 /Q5AX/ ;
3. .024 /L9/ ;
5. .176 .279 52.5 /Q6AX/ ;
3. .1945 /L10/ ;
13. 1.0 ;
-10. 2.0 1.0 .0 .001 /HWB/ ;
-10. 4.0 3.0 .0 .001 /VWB/ ;
-10. 1.0 1.0 5 .001 /HGB/ ;
-10. 3.0 3.0 5 .001 /VGB/ ;
3. .425 /L11/ ;
19. .2 2.056 /L1AX/ ;
3. .02 /L12/ ;
19. .2 -2.056 /L2AX/ ;
3. .365 /L13/ ;
-10. 2.0 1.0 .0 .001 /HWS/ ;
```

```
-10. 4.0 3.0 .0 .001 /VWS/ ;
-10. 1.0 1.0 5.5 .001 /HGS/ ;
-10. 3.0 3.0 5.5 .001 /VGS/ ;
SENTINEL (the data for a given problem is terminated by the word SENTINEL)
/FIT 6/ (fitting the data to the computer program TRANSPORT)
-1 (Indicator card: means the data that follows describes changes to be made in the previous
    problem)
19.00 /L8H/ ;                          (fix L8H together with their fitting constraint HWA2 &
                                        VWA2)
-10. /HWA2/ ;
-10. /VWA2/ ;
5.0A 'Q1AX' ;5.0B 'Q2AX' ;5.0A 'Q3AX' ;  (fit Q1AX, Q2AX, Q3AX, Q4AX,Q5AX & Q6AX
5.0A 'Q4AX' ;5.0B 'Q5AX' ;5.0A 'Q6AX' ;   with fitting constraint HGB & VGB, making sure
-10. /HWB/ ;                            that the fields of Q1AX, Q3AX, Q4AX & Q6AX and
10. /VWB/ ;                             Q2AX & Q5AX changes by the same amount)
10. 1.0 1.0 5 .001 /HGB/ ;
10. 3.0 3.0 5 .001 /VGB/ ;
SENTINEL
/FIT 7/
-1
5.00 'Q1AX' ;5.00 'Q2AX' ;5.00 'Q3AX' ;   (fix Q1AX, Q2AX, Q3AX, Q4AX, Q5AX, Q6AX
5.00 'Q4AX' ;5.00 'Q5AX' ;5.00 'Q6AX' ;    with their fitting constraint HGB & VGB)
-10. 'HWB' ;
-10. 'VWB' ;
-10. 'HGB' ;
-10. 'VGB' ;
19.0A  'L1AX' ;                         (fit L1AX with fitting constraint HGS & VGS)
19.0-A 'L2AX' ;
-10. 'HWS' ;
-10. 'VWS' ;
10. /HGS/ ;
10. /VGS/ ;
SENTINEL
/*PLOT*/ (plotting the TRANSPORT run to view the fitted beam envelope)
-1
19.00 'L1AX' ;
19.00 'L2AX' ;
-10. 'HWS' ;
-10. 'VWS' ;
-10. 'HGS' ;
-10. 'VGS' ;
SENTINEL (the data for a given problem is terminated)
SENTINEL (a second SENTINEL signifies the end of the TRANSPORT run)
```

NOTE THAT:

- Each element is given by a sequence of items, mostly numbers that are separated by spaces and terminated by a semicolon, which is a requirement to run TRANSPORT. The items, in order, are a type code number, a vary field, the physical parameter, and an optional label.
- The comments given in the appendix are merely stated to explain the meaning of the different elements in the beam card, and are not required when running the program.

APPENDIX C

TRANSPORT INPUT FILE USED FOR THE VAN DE GRAAFF BEAM EMITTANCE MEASUREMENTS (6 MV) IS HENCEFORTH LISTED:

/ Van de Graaff beamline 6 MeV: Emittance Measurements/

```
0 (Indicator card: means the data that follows describes a new problem)
13. 48.0 /ANG/ ;                    (Bending magnet input specification
15. 1.0 /mm/ 0.1 ;                  (Input-output units)
16. 14.0 0.0 /SLIT/ ;               (Print slit apertures)
-16. 31. 0. ;                       (Switch to random search algorithm)
13. 6. ;                            (Transformation matrix will be printed after every
                                     physical element that follows this code)
-16. 31. 0. ;                       (Switch to random search algorithm)
1. 1 3 1 3 .627 0.0 0.047469 /B1/ ; (Guess of initial beam parameters)
12. .0 .0 .0 .0 .0 .0 .0 .0 .0 .0 .0 .0 .0 .0 .0 /C1/; (Correlations beam matrix)
16. 3.0 1836.108 /MASS/ ;           (Mass of the particles comprising the beam, in units
                                     of electron mass)
 3. 2.17 ;                          (Drift space)
 2. 27 ;                            (Entrance edge angle: Pole face rotation)
 4. 1.037 90 0.0 /B90/ ;            (90^0 bending magnet)
 2. 5 ;                             (Exit edge angle: Pole face rotation)
 3. .810 /slit/;                    (Drift space at the slit)
-10. 1.0 1.0 1.25 .1 /F3/ ;         (Fitting constraint at the slits)
3. 1.178 ;                          (Drift space)
-10. 3.0 3.0 6.3828 .1 /F1/;        (Fitting beam size to y_max=6.3828mm)
-10. 1.0 1.0 3.7855 .1 /F2/;        (Fitting beam size to x_max=3.7855mm)
```

[The data that follows below has the same meaning as the one above, but with the edge angles and fitting constraint being different, i.e. the simultaneous multi envelope fitting.]

```
1. 1 3 1 3 .627 0.0 0.047469 /B6/ ;
12. .0 .0 .0 .0 .0 .0 .0 .0 .0 .0 .0 .0 .0 .0 .0 /C6/;
16. 3.0 1836.108 /MASS/ ;
 3. 2.17 ;
 2. 27 ;
 4. 1.037 90 0.0 /B90/ ;
 2. 30 ;
 3. .810 /slit/ ;
-10. 1.0 1.0 1.25 .1 /F3/ ;
 3. 1.178 ;
-10. 3.0 3.0 4.3797 .1 /F1/;
-10. 1.0 1.0 2.7061 .1 /F2/;

1. 1 3 1 3 .627 0.0 0.047469 /B7/ ;
12. .0 .0 .0 .0 .0 .0 .0 .0 .0 .0 .0 .0 .0 .0 .0 /C7/;
16. 3.0 1836.108 /MASS/ ;
 3. 2.17 ;
 2. 27 ;
 4. 1.037 90 0.0 /B90/ ;
 2. 35 ;
```

```
 3. .810 /slit/ ;
-10. 1.0 1.0 1.25 .1 /F3/ ;
 3. 1.178 ;
-10. 3.0 3.0 4.4114 .1 /F1/;
-10. 1.0 1.0 2.9139 .1 /F2/;

1. 1 3 1 3 .627 0.0 0.047469 /B10/ ;
12. .0 .0 .0 .0 .0 .0 .0 .0 .0 .0 .0 .0 .0 .0 .0  /C10/;
16. 3.0 1836.108 /MASS/ ;
 3. 2.17 ;
 2. 27 ;
 4. 1.037 90 0.0 /B90/ ;
 2. 25 ;
 3. .810 /slit/ ;
-10. 1.0 1.0 1.25 .1 /F3/ ;
 3. 1.178 ;
-10. 3.0 3.0 3.6552 .1 /F1/;
-10. 1.0 1.0 2.1041 .1 /F2/;

1. 1 3 1 3 .627 0.0 0.047469 /B11/ ;
12. .0 .0 .0 .0 .0 .0 .0 .0 .0 .0 .0 .0 .0 .0 .0  /C11/;
16. 3.0 1836.108 /MASS/ ;
 3. 2.17 ;
 2. 27 ;
 4. 1.037 90 0.0 /B90/ ;
 2. 20 ;
 3. .810 /slit/ ;
-10. 1.0 1.0 1.25 .1 /F3/ ;
 3. 1.178 ;
-10. 3.0 3.0 3.7818 .1 /F1/;
-10. 1.0 1.0 2.2080 .1 /F2/;

1. 1 3 1 3 .627 0.0 0.047469 /B12/ ;
12. .0 .0 .0 .0 .0 .0 .0 .0 .0 .0 .0 .0 .0 .0 .0  /C12/;
16. 3.0 1836.108 /MASS/ ;
 3. 2.17 ;
 2. 27 ;
 4. 1.037 90 0.0 /B90/ ;
 2. 15 ;
 3. .810 /slit/ ;
-10. 1.0 1.0 1.25 .1 /F3/ ;
 3. 1.178 ;
-10. 3.0 3.0 4.1947 .1 /F1/;
-10. 1.0 1.0 2.3369 .1 /F2/;

SENTINEL (the data for a given problem is terminated by the word SENTINEL)
 /FIT 1/ (fitting the data to the computer program TRANSPORT)
-1 (Indicator card: means the data that follows describes the changes to be made in the
    previous step of a given problem)
1.ABCD /B1/ ;                    (Coupled variation of x, θ, y and φ of the beam on all 5
1.ABCD /B6/ ;                    sections of fitting the beam parameters)
1.ABCD /B7/ ;
1.ABCD /B10/ ;
1.ABCD /B11/ ;
1.ABCD /B12/ ;
10. /F3/ ;                       (Fit F1, F2 and F3 now)
10. /F1/ ;
10. /F2/ ;
```

```
SENTINEL
/FIT 2/
-1
12.E0000F /C1/ ;
12.E0000F /C6/ ;
12.E0000F /C7/ ;
12.E0000F /C10/ ;
12.E0000F /C11/ ;
12.E0000F /C12/ ;
1. /B1/ ;
1. /B6/ ;
1. /B7/ ;
1. /B10/ ;
1. /B11/ ;
1. /B12/ ;

SENTINEL
/*PLOT*/ (plotting the TRANSPORT run to view the fitted beam envelope)
-1
1.ABCD /B1/ ;
1.ABCD /B6/ ;
1.ABCD /B7/ ;
1.ABCD /B10/ ;
1.ABCD /B11/ ;
1.ABCD /B12/ ;
SENTINEL
SENTINEL
```

(Vary r_{12} and r_{34} of the correlation matrix on all 6 sections of fitting the correlation beam matrix)

(Freeze or put constraint on x, θ, y and ϕ on all 6 sections)

(Coupled variation of x, θ, y and ϕ of the beam on all 6 sections of the beam parameters while r_{12} and r_{34} stays free)

NOTE THAT:

- Each element is given by a sequence of items, mostly numbers that are separated by spaces and terminated by a semicolon, which is a requirement to run TRANSPORT. The items, in order, are a type code number, a vary field, the physical parameter, and an optional label.
- This TRANSPORT run is a simultaneous multi envelope fit in which several sets of measured profile data are fitted. In this case six TRANSPORT run were fitted.
- The comments given in the appendix are merely stated to explain the meaning of the different elements in the beam card, and are not required when running the program.

APPENDIX D

THE TRANSPORT INPUT FILE USED FOR THE DESIGN OF THE VAN DE GRAAF +30^0 (SAFARI LINE) BEAMLINE (6 MeV) IS HENCEFORTH LISTED:

/VAN DE GRAAF +30^0 (SAFARI LINE) BEAMLINE 6 MeV /

```
 0 (Indicator card: means the data that follows describes a new problem)
 13. 48.0 /ANG/ ;                    (Bending magnet input specification)
 15. 1.0 /mm/ 0.1 ;                  (Input-output units)
 1. 2.2595 1.439 4.859 3.340 0.627 0.0 0.10628 ;(initial beam parameters)
 12. -0.861 0. 0. 0. 0. -0.883;      (Correlations beam matrix)
 16. 7.0 .7 ;                        (fringe field correction coefficient of bending magnet)
 16. 7.0 .45 ;                       (fringe field correction coefficients)
 16. 8.0 2.8 ;                  (for an unclamped "Regowski" fringing field boundaries)
 13. 1.;                             (current beam matrix printed here)
 13. 3.;                             (beam matrix printed after every physical element)
 3. .109 /L1/;                       (drift space)
 5.01 .110 -1.50 22.5 /Q1/ ;         (quadrupole 1)
 3. .085 /L2/;
 13. 1.;
 5.01 .110 1.50 22.5 /Q2/ ;
 3. .440 /L3/;
 10. 1. 1. 1. .001 /F1/ ;            (fitting constraint for parallel to point focus, horizontal
 10. 3. 3. 1. .001 /F2/ ;            ,F1, & vertical ,F2, planes for Q1 & Q2)
 3. 1.320 /L4/;
 16. 5.0 13.4 ;                      (vertical half-aperture of bending magnet, gap)
 20. -90.0 ;                         (beam angle of rotation in degrees)
 2. 27.0 /EA1/ ;                     (angle of pole-face rotation, degrees)
 4. 1.0374 90. .0 /D90/ ;            (90^0 bending magnet)
 2. 30.0 /EA2/ ;
 20. 90.0 ;
 3. 1.320 /L5/;
 3. .370 /L6/;
 5.0A .196 -0.150 25 /Q3/ ;
 3. .103 /L7/;
 5.00 .196 0.150 25 /Q4/ ;
 3. .103 /L8/;
 5.0A .196 -0.150 25 /Q5/ ;
 3. .229 /L9/;
 2. .0 ;
 4. 0.604 16. .0 /SWM/ ;             (switching magnet at 16^0)
 2. .0 ;
 3. 2.403 /L10/ ;
-10. 1. 1. 4. .001 /F3/;
-10. 3. 3. 10. .001 /F4/;
 5.00 .196 -0.20 25 /Q6/ ;
 3. .128 /L11/ ;
 5.00 .196 0.20 25 /Q7/ ;
 3. 1.85 /L12/ ;
-10. 1. 1. 1. .001 /F5/;
-10. 3. 3. 1. .001 /F6/;
```

SENTINEL *(the data for a given problem is terminated by the word SENTINEL)*
/FIT 1/ *(fitting the data to the computer program TRANSPORT)*
1 *(Indicator card: means the data that follows describes changes to be made in the previous problem)*

5.00 /Q1/;	(fix Q1 & Q2 together with their fitting constraint F1 & F2)
5.00 /Q2/;	
-10. /F1/;	
-10. /F2/;	
5.0A /Q3/;	(fit Q3, Q4 & Q5 with fitting constraint F3 & F4, making sure that the field of Q3 & Q5 changes by the same amount while fixing Q6 & Q7)
5.01 /Q4/;	
5.0A /Q5/;	
5.00 /Q6/;	
5.00 /Q7/;	
10. /F3/;	
10. /F4/;	
SENTINEL	
/FIT 2/	
1	
5.00 /Q3/;	(fix Q3, Q4 & Q5 together with their fitting constraint F3 & F4)
5.00 /Q4/;	
5.00 /Q5/;	
-10. /F3/;	
-10. /F4/;	
5.01 /Q6/;	(*fit Q6 & Q7 with fitting constraint F5 & F6 while* fixing Q3, Q4 & Q5)
5.01 /Q7/;	
10. /F5/;	
10. /F6/;	
SENTINEL	

/*PLOT*/ (plotting the TRANSPORT run to view the fitted beam envelope)
1
SENTINEL (the data for a given problem is terminated)
SENTINEL (a second SENTINEL signifies the end of the TRANSPORT run)

NOTE THAT:

- Each element is given by a sequence of items, mostly numbers that are separated by spaces and terminated by a semicolon, which is a requirement to run TRANSPORT. The items, in order, are a type code number, a vary field, the physical parameter, and an optional label.
- The comments given in the appendix are merely stated to explain the meaning of the different elements in the beam card, and are not required when running the program.

REFERENCE

BOT87 Botha A H, Burger S J, du Toit Z B, Reitmann D, Celliers P J, Cronje P M and Jungwirth H N, An injector cyclotron for acceleration of polarised and heavy ions at the NAC, Proc. 11th Int. Conf. On Cyclotrons and their Applications, Ionics, Tokyo (1987) p.515.

BRO67 Brown K L, Some first- and second-order magnetic optics theorems applicable to the design of beam transport systems and charged particle spectrometers. 2nd International Conference On Magnet Technology (1967) p.40.

BRO77 Brown K L and Rothacker F, Transport appendix, (1977), p.153.

BRO81 Brown K L, Beam envelope matching for beam guidance system. In "Charged particle optics" (H. Wollnik ed.). Nuclear Instruments and Methods 187 (1981) p.51.

CAR72 Carey D C, Computer simulation of charged particle beams. Nuclear Instruments and Methods 104 (1972) p.173.

CAR73 Carey D C, Minimization of aberrations in beam line design. IEEE NS-20 (1973) p.493.

CAR81 Carey D C, High-energy charged particle optics computer programs. In "Charged particle optics" (H. Wollnik ed.). Nuclear Instruments and Methods 187 (1981) p.97.

CAR98 Carey D C, Brown K L and Rothacker F, Third order TRANSPORT with MAD input. A computer program for designing charged particle beam transport systems, (1998).

CHA98 Chao A W and Tigner M, Handbook of accelerator physics and engineering. World Scientific Publishing Co. Pte. Ltd. (1998) p.58.

CON85 Conradie J L and Cornell J C, Die ontwerp van stuurmagnete vir hoe- en lae-energiebundellyne. Internal Report. NAC/85-09. National Accelerator Centre, NAC (1985).

CON92 Conradie J L, Improved proton beam quality and intensity from a 200 MeV cyclotron system. Ph.D.thesis, Physics Department, University of Stellenbosch, (1992).

DAV83 Davies W G, Introduction to first order optics (Chalk River Nuclear Laboratories), Canada KOJ 1JO (1983). AECL – 8053

DRA79 Dragt A J, A method of transfer maps for linear and nonlinear beam elements. IEEE Transactions on Nuclear Science, NS-26 (1979) p.3601.

DUT87 Du Toit Z B, Celliers P J, Roels L M M, Conard E P, Kritzinger J J and Burger S J, Operating experience with the light-ion injector of the NAC, Proc 11th Int. Conf. On Cyclotrons and Their Applications, Ionics, Tokyo (1987) p.109-112.

EMM63 Emmerson J McL and Middlemas N, Symmetry properties in beam transport systems. Nuclear Instruments and Methods 24 (1963) p.93.

GOL50 Goldstein H, "Classical Mechanics", Addison-Wesley publishing company, Inc. (1950) p.231.

HEN74 Hendrie D L, Magnetic detection of charged particles. In "Nuclear spectroscopy and reactions Part A" (J Cerny ed.). Academic Press, New York and London (1974) p.366.

KRO68 Kroon D J, "Laboratory magnets". Philips Technical Library, Eindhoven (The Netherlands), (1968) p.43.

LIV69 Livingood J J, The optics of dipole magnets, Academic Press, New York and London, 1969.

MER80 Merry C M and Cornell J C, Charged particle beam transport for a cyclotron facility. Internal Report. NAC/BT/80-01. National Accelerator Centre, NAC (1980).

MOK02 Mokoduwe P S, Conradie J L and de Villiers J G, Development of a duoplasmatron ion source at the iThemba LABS. M.Sc.thesis, Centre for Applied Radiation Science and Technology, University of North-West, (2002).

NAC76 National Accelerator Centre – Technical report of the Accelerator Task Group (National Accelerator Project) 1976.

PAR76 Parzen G, "Magnetic fields for transporting charged beams", Brookhaven National Laboratory, Associated Universities, Inc. (1976) p.8, 15.

PBO2.0 Particle Beam Optics Laboratory. PBO Lab™ 2.0 User Manual Supplement: TRANSPORT Application Module.

PEN61 Penner S, Calculations of properties of magnetic deflection systems. The Review of Scientific Instruments 32 (1961) p.150.

SPE67 Spencer J E and Enge H A, Split-pole magnetic spectrograph for precision nuclear spectroscopy. Nuclear Instruments and Methods 49 (1967) p.181.

STE65 Steffen K G, High Energy Beam Optics. Interscience monographs and texts in physics and astronomy, Volume XVII (1965) p.161.

WWW1 http://www.vector-fields.co.uk/tosca.html